Project of Strategic Interest NEXTDATA

Deliverable D2.6.3
Results of the Pilot Studies

Author: Elisa Palazzi
CNR ISAC, Torino

D2.6.3a: Analysis of water resources in the Himalaya-Karakoram and interaction between monsoon and mid-latitude perturbations

Author: Elisa Palazzi
CNR-ISAC, Torino

Contributors:
S. Terzago, L. Filippi, J. von Hardenberg
CNR-ISAC, Torino

A. Provenzale
CNR-IGG, Pisa

1. Introduction

The Hindu Kush–Karakoram (HKK) range, encompassing parts of Afghanistan, Pakistan, India, and China, is at the western edge of the Himalayan range. The whole Himalayan region is exposed to three main circulation patterns—the Indian summer monsoon, the East Asian monsoon, and westerly perturbations, also called western weather patterns (WWPs) (Archer and Fowler, 2004; Syed et al., 2006; Yadav et al., 2012; Pal et al., 2014)—leading to different precipitation climatologies in the western, central, and eastern portions of the mountain chain (Bookhagen and Burbank, 2010). The HKK in the west is strongly impacted by westerly perturbations originating from the Mediterranean/Atlantic regions during winter and it is affected, at least in part, by the monsoon during summer. As a result, precipitation in the HKK is characterized by a bimodal annual cycle (Palazzi et al., 2013).

Recently, the North Atlantic Oscillation (NAO) has been indicated as an important regulating factor in the Karakoram region (Syed et al., 2006; Yadav et al., 2009b). In particular, previous studies agreed in showing that winter precipitation in the Karakoram and the NAO are correlated with above (below) normal precipitation over the HKK area during the positive (negative) NAO phase. Moreover, the relationship between the NAO and precipitation in the HKK underwent secular variations during the twentieth century. Yadav et al. (2009b) investigated the temporal evolution of this relationship, finding significant correlations between the NAO and precipitation in the period from 1940 to 1980 and nonsignificant ones in the first and last part of the century. The recent drop in the NAO control was accompanied by a simultaneous strengthening of the relationship between El Niño– Southern Oscillation (ENSO) and precipitation in this area, which was not significant in the period 1940–1980. However, it is not clear if the secular variations in the NAO–precipitation relationship can be attributed entirely to changes in the intensity of the ENSO signal. Wang et al. (2012) introduced a new climate index [the angle index (AI)] to quantify the relative position of the NAO Centers Of Actions (COAs) in 20-yr running windows and showed that the AI provides additional information that cannot be represented by a standard, fixed-in-space NAO index.

In this Pilot Study we have investigated the relationship between the NAO and precipitation in the HKK region using three gridded archives based on the interpolation of in situ rain gauge measurements [the Global Precipitation Climatology Centre (GPCC), Climate Research Unit (CRU), and Asian Precipitation Highly- Resolved Observational Data Integration Toward Evaluation of Water Resources (APHRODITE) datasets] and the 40-yr European Center for Medium-Range Weather Forecasts (ECMWF) Re-Analysis (ERA-40). We opted for a multidataset approach to estimate the differences that could arise in the representation of this signal by using different large-scale data archives. We focused on the processes that are responsible for the link between the NAO and precipitation in the HKK. Particular emphasis is given to the study of the NAO-associated changes in evaporation from the main moisture reservoirs, which can help provide a more complete view of the whole mechanism. We also addressed the secular variations that occurred in the NAO–precipitation signal and investigated whether the spatial shifts in the NAO variability help us to understand the observed changes, using Twentieth Century Reanalysis (20CR) data (Compo et al., 2011) to reconstruct the atmospheric variability from 1871 to the present.

2. NAO–precipitation signal

We have explored the correlation between the NAO and precipitation by plotting the spatial distribution of the statistically significant correlations (at the 95% confidence level) between DJFM precipitation and DJFM NAOI time series (see Fig. 1) during the period 1958–2002. The strongest signal emerging from these plots is the well known European precipitation dipole, but another area displaying statistically significant positive correlations is located at the border between northeastern Pakistan and northwestern India, corresponding to the HKK region (although differences in the spatial extent arise between the datasets).

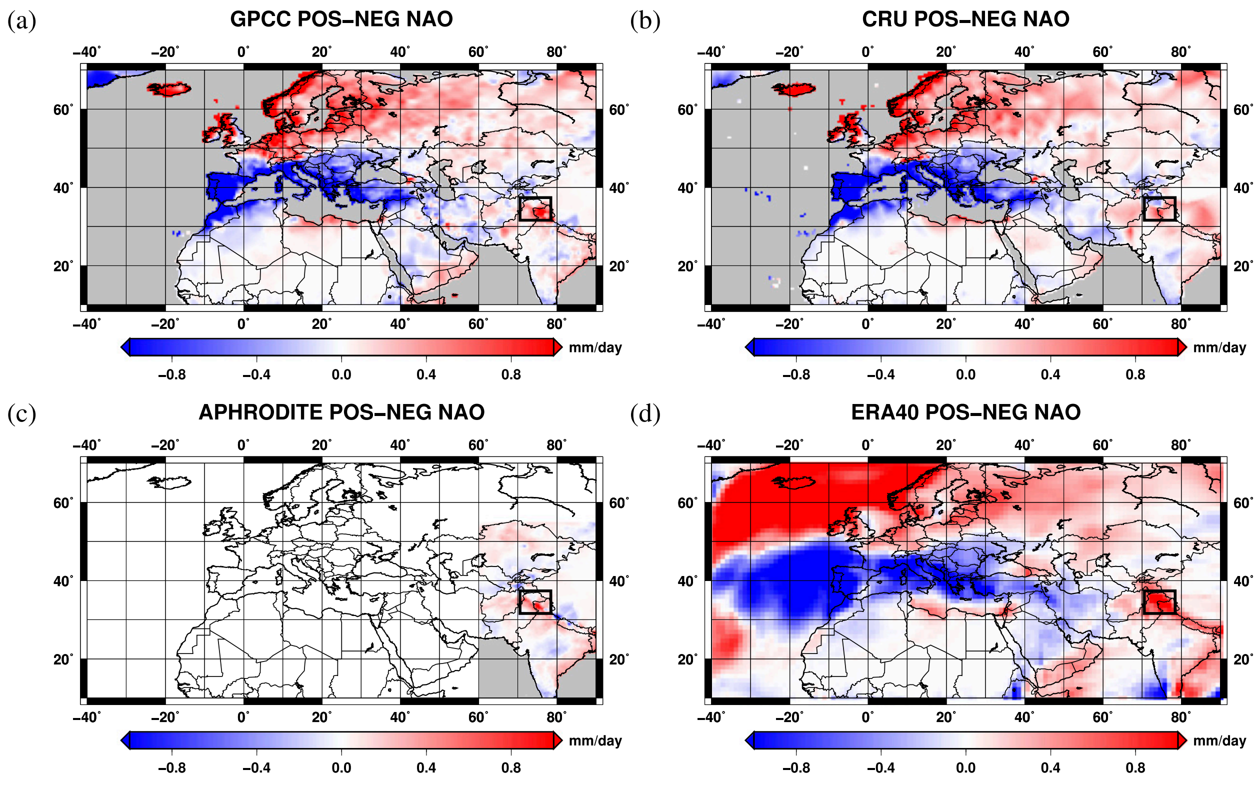

Fig. 1. Difference between the positive and the negative NAO composites of winter precipitation from (a) GPCC, (b) CRU, (c) APHRODITE, and (d) ERA-40 during the period 1958–2002. The black rectangle highlights the HKK region.

In the three observation derived datasets (GPCC, CRU, and APHRODITE) significant correlations are limited to a very small area and the weakest signal is found in CRU. Conversely, ERA-40 shows significant positive correlations over a broad area encompassing central and northern Afghanistan and Pakistan, and the greater Himalayan chain. Differences between the datasets highlight current problems in having reliable precipitation estimates in this region and the importance of using multiple datasets to estimate uncertainties. The lower correlation signal in station-based datasets, compared to ERA-40, may be associated with the underestimation of total precipitation in the observations (Palazzi et al., 2013) where winter snowfall is not adequately captured. However, we note that reanalysis precipitation outputs should be treated with care, as they are susceptible to model errors and inhomogeneities in the data used in the assimilation procedure.

3. NAO-related variability of moisture transport and evaporation

To study the effects of the NAO on tropospheric westerlies over the HKK region, in the vertical cross section of Fig. 2 we show the correlation coefficients between the NAO Index and zonal wind (averaged between 40° and 70°E) in the Northern Hemisphere. This meridional band corresponds to the longitudes of greater importance for the transport of humidity toward the HKK. Significant positive correlations are found from the lower to the higher troposphere at latitudes between 20° and 30°N, where the climatological jet stream is located. The jet stream core in the upper troposphere (around 200hPa) is intensified and slightly shifted to the north during the positive NAO phase. The strengthening of the westerlies at these latitudes is marked throughout the troposphere and weakens slightly only at lower levels (below 800–850 hPa), where surface effects become important.

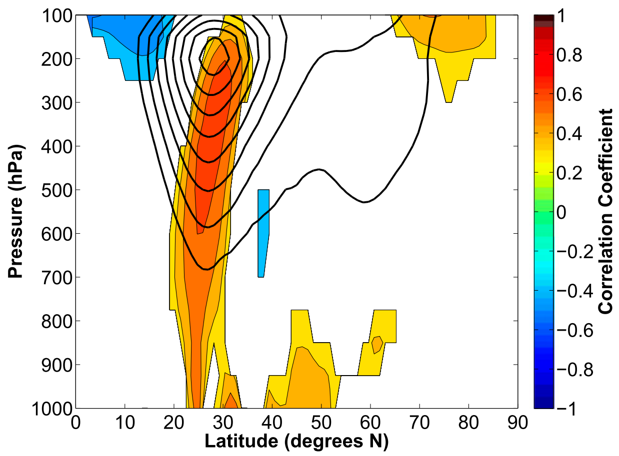

Fig. 2. Correlation coefficients (filled colored contours) between the NAOI and winter zonal wind averaged over longitudes between 408 and 708E during the period 1958–2002. Only correlations statistically significant at the 95% confidence level are reported. Climatology (1958–2002) of winter zonal wind (black contours) averaged over longitudes between 408 and 708E, identifying the position of the Middle East jet stream: only values above 10 m/s are reported. Contour interval is 5 m/s.

We explore to what extent this anomaly in westerly winds affects moisture transport toward the HKK. A first step is to identify the major sources of the humidity transported to the HKK region. We found that moisture, originating mainly from the northern Arabian Sea and the Red Sea, is transported toward the HKK through the Persian Gulf. A comparatively smaller moisture contribution comes from the Mediterranean area, although, on average, moisture from that area deviates northeastwardly and affects mainly the regions north of the HKK. The intensity of moisture transport from the Arabian Peninsula toward Pakistan and western India is significantly larger during the positive NAO phase. The strengthening of moisture transport in this region during the positive NAO phase may sustain wetter than normal conditions in winter in the HKK (Filippi et al., 2014). Wind is not the only variable influencing moisture transport: during the positive NAO phase, enhanced evaporation occurs from the Red Sea, the Persian Gulf, the northern Arabian Sea, and the southeastern Mediterranean Sea.

These basins constitute the major moisture sources for the HKK. The evaporation signal from the Red Sea, the Persian Gulf, and the northern Arabian Sea is associated with coherent signals in surface wind speed and SST. Our results (Filippi et al., 2014) suggest that the dominant path through which the NAO induces higher evaporation is the intensification of surface winds. This intensification might ensue from the NAO-induced strengthening of tropospheric westerlies over this region (see Fig. 2), although the link between the two is not trivial given the strong influence of surface conditions.

4. Nonstationarity of the NAO–precipitation teleconnection

In Fig. 3 we show the sliding correlations over 21-yr moving windows between the NAOI and the time series of precipitation averaged in the HKK domain from GPCC, CRU, APHRODITE, and ERA-40. The HKK domain is defined, as in Palazzi et al. (2013), in the range 32°–37°N, 71°–78°E. The various datasets have different temporal coverages, but they all show consistent changes in the NAO–precipitation relationship during their overlapping periods. Correlation coefficients between the NAO and precipitation are significant in the period between 1940 and 1980, whereas they are not significant after 1980 and between 1920 and 1940. The two datasets extending to the first years of the twentieth century show a stronger signal before 1920 with respect to the following decade (the correlations are statistically significant in CRU but not in GPCC) and seem to suggest a decline of the NAO control on precipitation during these years. However, it is worth pointing out that precipitation estimates are less and less reliable as we move back to the beginning of the century, as the number of stations in this area decreases and the gridded datasets are obtained by interpolating data from stations quite far from each other.

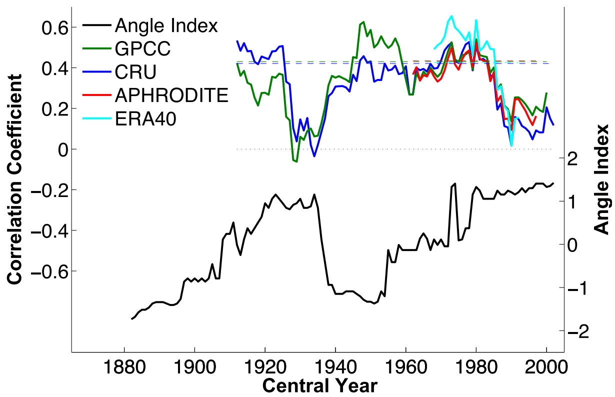

Fig. 3. Sliding correlations on 21-yr moving windows between the NAOI and the time series of precipitation averaged in the HKK domain (71°–78°N, 32°–37°E) from GPCC (green), CRU (blue), APHRODITE (red), and ERA-40 (cyan). Dashed lines indicate the 95% significance level and the dotted line indicates zero correlation. The black line is the time series of the AI. Sliding correlations and the AI have different y axes on the left and right side respectively. Values are plotted at the 11th year of each 21-yr window.

Figure 3 shows the time series of the angle index, which measures the spatial displacements of the NAO pattern in the North Atlantic on decadal time scales. The temporal evolution of the AI shows interesting similarities with the time series of the correlation between the NAO and precipitation, and the two seem to evolve in antiphase: in the two periods with non-significant correlations (1920–40 and 1980 onward) the AI shows the highest values (i.e., the NAO has a positive tilt). Conversely, the period with significant correlations (1940–1980) is characterized by lower values of the AI, which was strongly negative before the mid-1950s (when GPCC shows its highest correlations) and approximately zero afterward. At the beginning of the twentieth century, when CRU and GPCC suggest a weakening of the NAO–precipitation relationship, the AI is moving from negative to positive values. There are sources of variability other than the NAO for precipitation in this area, and these factors add noise to the record of sliding correlations, potentially worsening the synchronization with the time series of the AI. Our results support the view that the position of the NAO COAs regulates the strength of the NAO–precipitation relationship in the HKK region. In particular, Fig. 3 suggests that, when the NAO has a positive tilt, the NAO–precipitation correlation is weaker, whereas suitable conditions for the NAO–precipitation correlation are found when the NAO shows a negative—or at least very small—tilt.

5. Discussion and conclusions

Winter precipitation in the Hindu Kush–Karakoram (HKK), an essential water input for the area, is associated with the arrival of westerly perturbations, the western weather patterns (WWPs), originating from the Mediterranean and northeastern Atlantic regions. The existence of correlations between the NAO and winter precipitation in the HKK is well known (Syed et al., 2006, 2010; Yadav et al., 2009b). Here we have used an ensemble of large-scale precipitation datasets, showing that they coherently reproduce the NAO–precipitation link, and we have discussed the importance of evaporation anomalies in the processes responsible for the relationship between the NAO and winter precipitation in the HKK. We have also addressed the issue related to the multidecadal variations occurring in the NAO–precipitation relationship and have argued that these changes are related to the spatial structure of the NAO pattern in the North Atlantic basin. Our analysis of the relationship between the NAO index and precipitation estimates from three gridded observation-based datasets and from the ERA-40 reanalysis confirms that the NAO influences the amount of precipitation in the HKK. All datasets considered here show that years in the positive (negative) NAO phase are characterized by above (below) normal precipitation over the target area in winter (December– March).

The relationship between precipitation and the NAO is maintained through the control exerted by the NAO on the westerlies in the region of the Middle East jet stream (MEJS), from North Africa to southeastern Asia. At longitudes between 40° and 70°E, where the majority of moisture transport toward the HKK takes place, the intensification of the westerlies during the positive NAO phase is evident from the upper-tropospheric jet to the lower-level westerlies. The stronger jet intensifies the WWPs and faster westerlies in the middle to lower troposphere intensify moisture transport toward the HKK. In addition to this, we have shown that evaporation plays an important role in this mechanism. Our analysis suggests that the main moisture sources for precipitation in the HKK are in the northern Arabian Sea, the Red Sea, the Persian Gulf, and, to a lesser extent, the Mediterranean Sea. During the positive NAO phase, enhanced evaporation occurs from these reservoirs. Evaporation anomalies from the first three basins are mainly related to higher surface wind speed. We suggest that surface wind anomalies might be associated with the strengthening of westerlies in this region during the positive NAO phase, even if the link with upper-level circulation is not trivial owing to the strong effects of surface topography. The increased humidity arising from evaporation combines with the intensification of westerlies to give enhanced moisture transport toward the HKK. As a consequence, wetter conditions are found over northern Pakistan and northern India and larger precipitation amounts are released as the western weather patterns reach this region. The precipitation datasets used in this study show significant multidecadal variations in the relationship between the NAO and precipitation. We have used the NAO angle index (AI) introduced by Wang et al. (2012) to measure the slow movements of the NAO centers of action. Our results show that high values of the AI (positive tilt of the NAO) are associated with nonsignificant correlations between the NAO and precipitation in the HKK, while significant correlations occur when the AI is negative. Shifts in the position of the NAO COAs have significant implications for the NAO-associated circulation anomalies in the troposphere. In particular, when the AI is low, the NAO exerts a strong control on the MEJS and, as a consequence, the mechanism of regulation of the HKK precipitation by the NAO is activated. The opposite occurs when the AI is high. The AI considered here is one of the possible indices measuring the changes in the NAO spatial pattern, and others can be defined that capture slightly different features (such as considering only one of the two centers of action). What is important here is that changes in the spatial structure of the NAO pattern can be crucial in determining the strength of the relationship between the NAO and other climatic parameters, and as a consequence in determining precipitation in the HKK.

References

ARCHER D. R., AND FOWLER H. J., (2004): Spatial and temporal variations in precipitation in the Upper Indus Basin, global tele- connections and hydrological implications. *Hydrol. Earth Syst. Sci*., 8, 47–61, doi:10.5194/hess-8-47-2004.

BOOKHAGEN B., AND BURBANK D. W., (2010): Toward a complete Himalayan hydrological budget: Spatiotemporal distribution of snowmelt and rainfall and their impact on river discharge. *J. Geophys. Res.*

COMPO G. P., and COAUTHORS, (2011): The Twentieth Century Re- analysis Project. *Quart. J. Roy. Meteor. Soc*., 137, 1–28, doi:10.1002/ qj.776.

FILIPPI L., PALAZZI E., VON HARDENBERG J., PROVENZALE A., (2014): Multidecadal Variations in the Relationship between the NAO and Winter Precipitation in the Hindu Kush–Karakoram, *Journal of Climate*, 27, 7890-7902, doi: 10.1175/JCLI-D-14-00286.1.

PAL I., ROBERTSON A. W., LALL U., AND CANE M. A., (2014, in press): Modeling winter rainfall in northwest India using a hidden Markov model: Understanding occurrence of different states and their dynamical connections. *Climate Dyn*., doi:10.1007/ s00382-014-2178-5.

PALAZZI E., VON HARDENBERG J., and PROVENZALE A., (2013): Precipitation in the Hindu-Kush Karakoram Himalaya: Observations and future scenarios. *J. Geophys. Res*., 118, 85–100, doi:10.1029/2012JD018697.

SYED F. S., GIORGI F., PAL J. S., and KING M. P., (2006): Effect of remote forcings on the winter precipitation of central south- west Asia. Part 1: Observations. *Theor. Appl. Climatol*., 86, 147–160, doi:10.1007/s00704-005-0217-1.

——, ——, ——, and K. KEAY, (2010): Regional climate model simulation of winter climate over central-southwest Asia, with emphasis on NAO and ENSO effects. *Int. J. Climatol*., 30, 220– 235, doi:10.1002/joc.1887.

WANG Y.-H., MAGNUSDOTTIR G., STERN H., TIAN X., and YU Y., (2012): Decadal variability of the NAO: Introducing an augmented NAO index. Geophys. *Res. Lett*., 39, L21702, doi:10.1029/2012gl053413.

YADAV R. K., RUPA KUMAR K., and RAJEEVAN M. (2009b): Increasing influence of ENSO and decreasing influence of AO/NAO in the recent decades over northwest India winter precipitation. *J. Geophys. Res*., 114, D12112, doi:10.1029/2008JD011318.

YADAV R. K, KUMAR K. R., and RAJEEVAN M., 2012: Characteristic features of winter precipitation and its variability over northwest India. *J. Earth Syst. Sci*., 121, 611–623, doi:10.1007/s12040-012-0184-8.

D2.6.3c: Estimation of the changes in the hydrological cycle, snow cover and water availability in high altitude areas.

Author: Silvia Terzago
CNR-ISAC, Torino.

Contributors: E. Palazzi, J. von Hardenberg
CNR-ISAC, Torino
A. Provenzale
CNR-IGG, Pisa
C. Cassardo
Univ. Torino, Dip. Fisica
U. Morra di Cella, E. Cremonese
ARPA-VdA.

This Deliverable is structured as follows: the introduction describes the objectives of the Present Pilot study which aims to explore the possibility of achieving accurate simulations of the snow pack characteristics and their temporal variability using two land surface models driven by data of different nature (i.e. surface observations, reanalyses) and different temporal resolution.
A section is dedicated to the description of (i) the land-surface models, including the input variables they require, (ii) the datasets used to drive the models and to validate the models output, and (iii) the different experiments we have carried out with the models.
Follows a section with the presentation of the results, and finally the conclusions with the discussion of the strengths and limitations of this study, and the perspectives for future work.

Introduction

The long-term objective of this Pilot Study is to provide information on the recent and future expected changes in snow resources and in the hydrological cycle in high altitude areas, with a focus on the Alps and Apennines.
A possible approach is to investigate future snow projections of Global Climate Models (GCMs) which provide information at large scale, with spatial resolution of the order of ~100 km. An advantage of this approach is the possibility to analyze and compare an ensemble of GCM snow outputs made available in the framework of the CMIP5 experiment (Taylor et al., 2012), and evaluate the spread among the model projections. As a drawback, snow processes in global climate models are strongly simplified and coarsely represented. In fact, the main purpose of snow schemes in the current generation of GCMs is to adequately represent snow covered area, surface albedo and surface temperature and provide a realistic forcing to the model's atmosphere component (Steger et al., 2013). This limitation causes high uncertainty in the future snow pack projections and melt-water availability (see i.e. Terzago et al., 2014).
The evaluation of the temporal and spatial changes of snow pack requires a highly resolved representation of the atmospheric and surface dynamics in mountain regions. To reach this goal, Global Climate Models can be dynamically downscaled using Regional Climate Models (RCMs), currently reaching resolutions down to 10 km and including a representation of surface processes at such scales. However, this resolution can still be too coarse for mountain areas with complex and steep topography. Recent studies suggest an alternative approach

consisting in using the atmospheric variables produced by global or regional climate models appropriately downscaled to drive land surface models able to simulate the temporal variability of snowpack characteristics at very local scale (e.g. Schmucki et al., 2014; Steger et al., 2013). In this case, the land surface model is run in off-line mode, so the surface-atmosphere feedbacks cannot be represented but, on the other hand, it is possible to represent the snow processes with higher detail, and presumably, with more accuracy.
Here we investigate this last approach, considering two land surface models, the European Centre for Medium-Range Weather Forecasts (ECMWF) Hydrology-Tiled ECMWF Scheme for Surface Exchange over Land (HTESSEL) and the University of TOrino land Process Interaction in Atmosphere (UTOPIA). The first aim is to determine how reliable they are in representing the temporal evolution of the snow pack in "optimal condition", i.e. when they are forced with high-quality and high frequency measurements. Secondly, as our focus is on reproducing snow variability on regional scale, both over the historical period and in future scenarios, we explore the possibility of driving the land-surface models with climate models simulations. To this objective, we investigate how the accuracy of the models drops when they are forced with low temporal resolution measurements and model data (reanalysis) with spatial resolution comparable to that of global/regional climate models.

Models, data, methods

Land-surface models

For our experiment we use two land-surface models, the Hydrology-Tiled ECMWF Scheme for Surface Exchange over Land (HTESSEL, Balsamo et al., 2011) and the University of TOrino land Process Interaction in Atmosphere (UTOPIA, Cassardo et al., 2014). Both models compute the land surface response to the atmospheric forcing, estimating the surface water and energy fluxes along with the temporal evolution of the snowpack, soil temperature, and moisture. The models simulate the snow water equivalent *swe*, the snow density ρ. The snow depth *sd* is derived from *swe* and ρ as

$$sd = swe\ \rho_w/\rho_{sn}$$

where ρ_w = 1000 kg/m^3 is the density of the liquid water.
The main variables needed to force the models are: near surface air temperature, total precipitation, wind direction and speed, relative humidity, surface pressure, shortwave and longwave incoming radiation. Some manipulation has been performed to adapt these variables to the models requirements, for example to address the fact that UTOPIA requires total precipitation, horizontal and vertical components of the surface wind while HTESSEL requires rainfall and snowfall components of precipitation, wind direction and speed.

Forcing and validation data

The forcing we used are:

- the meteorological measurements of the high elevation station of Torgnon (45°N, 34°W, 2160 m a.s.l) located in Aosta Valley, Western Italian Alps, measuring all the input variables needed to force the models at high frequency and with high level of accuracy. This station is operational with full equipment since mid-2012 so we consider the dataset over the period June 1st 2012 - July 31st 2014.
- ERA-Interim reanalysis (Dee et al., 2012), a global gridded data product providing 3-hourly surface parameters describing atmospheric and land-surface conditions. ERA-Interim grid has resolution of 0.75° in longitude and latitude, implying a smooth topography and coarse scale representation of physical processes, as in the case of global climate models.

The former dataset allows to test the models in the condition of "optimal forcing", i.e. when all input variables are measured with high degree of accuracy. The latter, ERA-Interim dataset, allows to explore the models response in the "extreme" condition when no surface data are availabile and coarse-scale model datasets, i.e. reanalyses, have to be used.
To validate the output continuous snow depth measurements obtained by the ultrasonic distance sensor at the Torgnon station have been used. Snow density measurements occasionally performed in winter and early spring seasons at the same station have been considered.

Experimental design

In order to verify the skill of the models and to test their sensitivity to changes in the spatial and temporal resolution of input data, we performed the following tests over the period June 1st 2012 - July 31st 2014:

- OBS: The first run of the models is performed using high quality meteorological forcing measured at the Torgnon weather station, at 30 minutes temporal resolution.
- OBS3, OBS6, OBS12: These experiments are performed using the meteorological measurements at intervals of 3, 6 or 12 hours. The data were interpolated to the time step of the land surface models, using linear interpolation for all variables except for precipitation, for which a constant precipitation rate is assumed over the 3, 6 or 12 hour time interval.
- ERA: The third experiment is performed forcing the models with the ERA-Interim reanalysis interpolated in time to the land surface models integration time step of 30 minutes.
- ERA-LR, ERA-BIAS: These experiments are similar to the previous one but we correct the ERA-Interim temperature using the local elevation at the site and the adiabatic lapse rate. ERA-Interim gridpoint nearest to the Torgnon weather station is 1480 m a.s.l., that is, 680 m lower than the true station altitude. In experiment ERA-LR we corrected the temperature data for the elevation, assuming a fixed moist lapse rate of 6.5°C/km. In experiment ERA-BIAS, we corrected the temperatures using the difference in the climatological averages between the temperatures reported by ERA and those measured at the Torgnon station. This bias was subtracted from the ERA-Interim temperature and was assumed to be constant in time. After the temperature correction, we recomputed the relative humidity from the dewpoint temperature and the 2-meter temperature.

Results

The first experiment (OBS) reveals the ability of the two land surface models HTESSEL and UTOPIA to reproduce the snowpack temporal evolution when optimal meteorological forcing is used, that is, high-quality measurements at 30-min temporal resolution. UTOPIA and HTESSEL reproduce fairly well the temporal evolution of the snow depth, with an underestimation of the snow peak in mid-spring. UTOPIA simulation is slightly closer to the observations, giving the smaller bias in the representation of the snow depth maximum. The root mean squared error (RMSE) conditioned to snow depth ≥ 0.01 m is 0.11 m for UTOPIA and 0.20 m for HTESSEL.
The second set of experiments (OBS3, OBS6 and OBS12) uses meteorological drivers obtained by linear interpolation (aggregation) of surface station measurements at 3, 6 and 12 hour

temporal resolution. The results of the simulations performed using 3 and 6 hourly data are comparable to that obtained in the run OBS with the 30 minute forcing. Poorer results are obtained with 12 hourly data as the inaccuracy in air temperature data does not allow to properly separate solid from liquid precipitation and a rough estimate of incoming shortwave radiation causes a poor reproduction of the energy budget. These problems result in an underestimation of snow accumulation and earlier start of the snow melting. This experiment shows that 6-hourly data are sufficient for a good reproduction of snowpack temporal variability and we do not loose accuracy using meteorological forcings up to 6 hour temporal resolution.

In the ERA runs, despite the coarse temporal and spatial resolution of the meteorological forcing, we observe a fairly good reproduction of the snow depth temporal variability. The depth of the snow mantle is correctly simulated by both models in winter/early spring when it is (i) comparable to the corresponding results obtained in OBS and OBS3,6,12 and (ii) very close to the observations. ERA runs reproduce an early snow depth maximum and an early melting that results in complete snow ablation several weeks earlier than observed. We observe that late spring and autumn snowfalls are often missed. This is due to the fact that the elevation of the ERA-Interim gridpoint is 680 m lower than the actual altitude of the station, thus ERA-Interim temperatures are generally higher than the observed ones and the separation between rainfall and snowfall on the basis of ERA-Interim temperature favours liquid with respect to solid precipitation.

In ERAI-LR runs, the reanalysis temperature data are corrected for elevation using a moist lapse rate at the Torgnon site. This correction solves the problem of early snow melting in late spring and it allows to identify late spring/autumn snow accumulation episodes. During the first Winter (2012-2013), this correction produces snowfall and snow depth overestimation for most of the season, for both models. During the second Winter season (2013-2014), instead, the correction provides an estimate of snow cover which is very close to observations.

The ERAI-BIAS run uses ERA-Interim temperature data corrected directly for the bias with respect to the observed temperature climatology. We observe a clear improvement of the models performances with respect to the non-adjusted ERA Interim data. The amplitudes of the snowfall events are correctly reproduced, as well as the snow depth peaks and the melting. During the first winter, this type of correction performs better than experiment ERAI-LR.

Conclusions

Both UTOPIA and HTESSEL models are able to capture fairly well the accumulation and melting processes and to reproduce the temporal evolution of the snowpack along the season, despite an underestimation the snow depth peak in spring. The experiments performed with meteorological drivers with degraded temporal resolution show that models accuracy is comparable if we use up to 6-hourly data linearly interpolated or disaggregated to the model time step (in this case 30'). The technique of forcing a land surface model with ERA-Interim fields corrected for the elevation of the site under study allows to obtain rather good performances and an overall good correspondence between the simulated snowfall/snow melting episodes and observations.

This experiment suggests that the snowpack characteristics and their temporal variability can be adequately simulated also when high spatial and temporal resolution surface observations are limited or not available, as it is often the case in high elevation areas. Coarse-grid atmospheric forcings such as reanalyses or climate model outputs, adequately corrected for elevation, can provide satisfactory input for snow models. Of course, these results have been obtained using a single measurement site and their validity is limited to that point location. Further steps will be to extend the analysis to other high-quality meteorological datasets, in order to draw more general conclusions.

References

BALSAMO G., BOUSSETTA S., DUTRA E., BELJAARS A., VITERBO P., and VAN DEN HURK B., (2011): Evolution of land surface processes in the IFS. ECMWF Newsletter, 127, 17–22.

CASSARDO C., (2006): The Land Surface Process Model (LSPM) version 2006. The complete manual. Università degli Studi di Torino, Dipartimento di Fisica Generale "A. Avogadro", dfg report - 01/2006 ed., URL http://goo.gl/jmzxss.

DEE D. P., and COAUTHORS, (2011): The ERA-Interim reanalysis: configuration and performance of the data assimilation system. *Quarterly Journal of the Royal Meteorological Society*, 137 (656), 553–597, doi:10.1002/qj.828, URL http://dx.doi.org/10.1002/qj.828.

SCHMUCKI E., MARTY C., FIERZ C., and LEHNING M., (2014): Simulations of 21st century snow response to climate change in Switzerland from a set of RCMs. *International Journal of Climatology*.

STEGER C., KOTLARSKI S., JONAS T., and SCHAR C., (2013): Alpine snow cover in a changing climate: a regional climate model perspective. *Climate dynamics*, 41 (3-4), 735–754.

TAYLOR K. E., STOUFFER R. J., and MEEHL G. A., (2012): An overview of CMIP5 and the experiment design. *Bulletin of the American Meteorological Society*, 93 (4), 485–498.

TERZAGO S., VON HARDENBERG J., PALAZZI E., and PROVENZALE A., (2014): Snowpack changes in the Hindu-Kush Karakoram Himalaya from CMIP5 Global Climate Models. *Journal of Hydrometeorology*, doi:10.1175/JHM-D-13-0196.1.

D2.6.3d: Effects of aerosols in high-altitude regions

Lead Author: Jost von Hardenberg
CNR-ISAC, Torino.

Contributors: E. Palazzi, S. Terzago
CNR-ISAC

The activites performed in this Pilot Study have been two-fold. On the one side, we have analysed the output of one regional climate model (the RegCM4 model run by ICTP) in terms of Aerosol Optical Depth (AOD) in the HKKH region and compared the model results with satellite observations (MODIS-Terra) and with an aerosol reanalysis product provided by the MACC Project (Monitoring Atmospheric Composition and Climate). On the other side, we have analysed the output of the historical (1870-2005) and scenario (2600-2100) simulations of thirty-two CMIP5 global climate models (GCMs) participating in the CMIP5 effort, in order to understand what model features, particulalrly those related to the aerosol properties, may affect the representation of seasonal precipitation in the HKKH region.

1. Regional simulations

Since these activities were carried out mainly during the first Project year as described carefully in the D2.6.1 Deliverable of the NextData Project, we will only resume here the most significant outcomes, by referring to the first year Deliverable for all other information related, e.g., to the model specifications, experiments, and configurations.

The RegCM4 model has been run for a regional domain including the Indian subcontinent defined for the CORDEX Project. Two present-day simulations (2000-2009) are available with boundary conditions provided by ERA-Interim reanalyses and by the global model EC-Earth run created for CMIP5 by CNR-ISAC. A future scenario timeslice in the period 2040-2050 has been also created using boundary conditions from the EC-Earth GCM for the RCP 4.5 emission scenario.

The spatial distributions of the AOD climatologies are reported in Fig. 1, averaged over the years 2003-2009, common to all datasets. These figures show that in winter RegCM is capable of reproducing to a large extent the amplitude and the spatial distribution of the optical depth of aerosols in this area, with a good reproduction of a low over the Tibetan plateau and of a higher AOD at the southern feet of the Himalayas, mainly associated with anthropic pollution. In summer we find a good reproduction of a severe maximum of AOD centered over the border between Pakistan and India, even if with an offset in the position of the maximum which is located farther west. Experimentation with a the dynamical dust scheme used in the model has allowed to assess the role of an accurate representation of dust emissions from the local desert areas (mainly the Thar desert) in order to represent correctly this maximum during the monsoon season. The figure compares the results for present-day conditions using the ERA-Interim reanalysis boundary conditions. Results with EC-Earth boundary conditions are very similar.

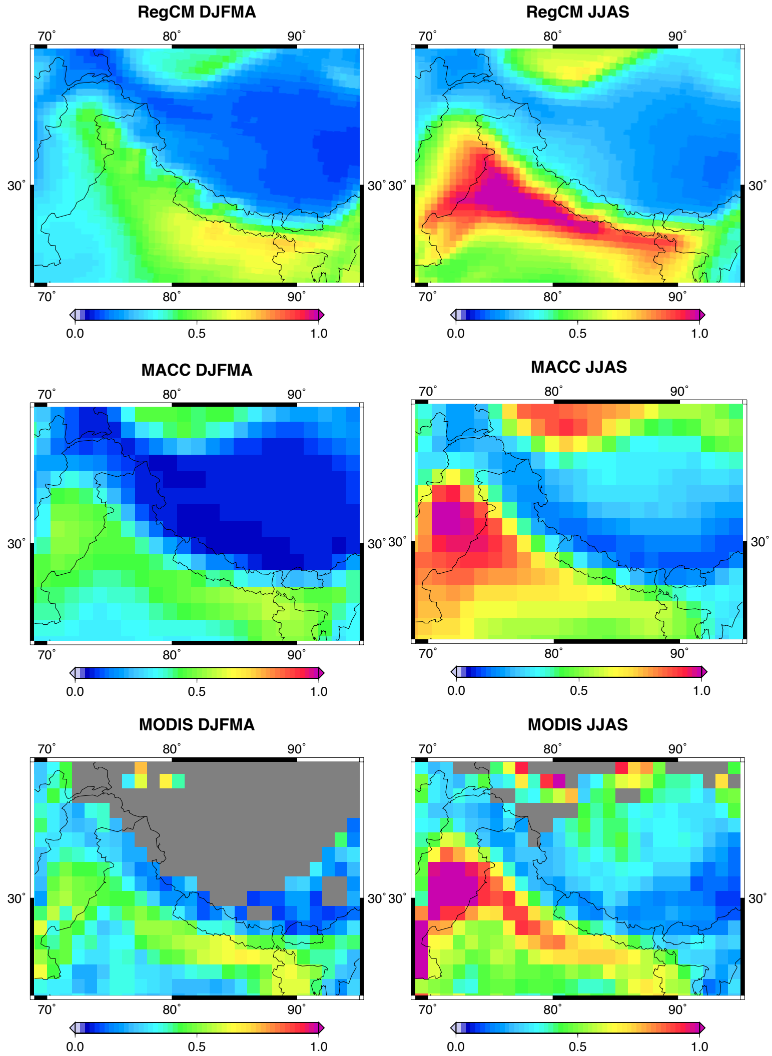

Fig. 1. Comparison over the HKKH of AOD in the visible band simulated by the RegCM4 model with Era-Interim boundary conditions (top row) with AOD (at 550 nm) reproduced by the MACC reanalysis (middle row) and by MODIS (bottom row). The left column refers to winter-early spring (DJFMA), the right one to the summer monsoon season (JJAS).

We also gained an insight on the ability of the model in reproducing AOD distributions over a wider region encompassing the whole Indian CORDEX domain (not shown here) in order to better analyse the role of long-range transport mechanisms. While large areas, characterized by high albedo, such as the desert areas of Arabia or over the Tibetan plateau in winter, cannot be measured correctly by Modis, we saw that the model presents a good correspondence in the large-scale distribution of AOD. Sulfate emissions in east-Asia appeared overestimated in the model, and through long range transport may contribute significantly to the presence of increased summer anthropogenic pollutants also over the HKKH. A significant close source area, not seen by Modis, of dust in summer was evident in the RegCM4 simulation over western China.

We finally analyzed deposition fluxes of light-absorbing aerosols, namely black carbon and dust. This analysis confirmed the importance of dust deposition mainly during the monsoon summer season on the southern flanks of the HKKH. The changes in these deposition fluxes in the RCP 4.5 future scenario (for 2040-2050) compared to present-day are highlighted a possible decrease in winter BC deposition, mainly associated with a decrease in the scenario of east-Asian anthropogenic emissions. The model also forecasts a significant decrease in dust activity affecting the Himalayas, both in summer (from the Thar desert) and in winter (from the Gobi desert).

2. Global simulations

We have analyzed the output of historical (1870–2005) and scenario (2006–2100) simulations of thirty-two models participating in the CMIP5 experiment, available from the Earth Science Grid Federation archive. The CMIP5 models used in this study, their horizontal and vertical spatial resolution, the representation of the aerosol indirect effects and key references are shown in Table 1.

Model ID	Resolution Lon × Lat° Lev	Institution ID	First/second indirect aerosol effect	Key reference
bcc-csm1-1-m	1.125 × 1.125L26 (T106)	BCC	No	Wu et al. (2013)
bcc-csm1-1	2.8125 × 2.8125L26 (T42)	BCC	No	Wu et al. (2013)
CCSM4	1.25 × 0.9L27 (T63)	NCAR	No	Meehl et al. (2012)
CESM1-BGC	1.25 × 0.9L27	NSF-DOE-NCAR	No	Hurrell et al. (2013)
*CESM1-CAM5	1.25 × 0.9L27	NSF-DOE-NCAR	No	Hurrell et al. (2013)
EC-Earth	1.125 × 1.125L62 (T159)	EC-EARTH	No	Hazeleger et al. (2012)
FIO-ESM	2.8125 × 2.8125L26 (T42)	FIO	No	Song et al. (2012)
GFDL-ESM2G	2.5 × 2L24 (M45)	GFDL	No	Delworth et al. (2006)
GFDL-ESM2M	2.5 × 2L24 (M45)	GFDL	No	Delworth et al. (2006)
MPI-ESM-LR	1.875 × 1.875L47 (T63)	MPI-M	No	Giorgetta et al. (2013)
MPI-ESM-MR	1.875 × 1.875L95 (T63)	MPI-M	No	Giorgetta et al. (2013)
*CanESM2	2.8125 × 2.8125L35 (T63)	CCCMA	Yes / No	Arora et al. (2011)
CMCC-CMS	1.875 × 1.875L95 (T63)	CMCC	Yes / No	Davini et al. (2013)
CNRM-CM5	1.40625 × 1.40625L31 (T127)	CNRM- CERFACS	Yes / No	Voldoire et al. (2013)
*CSIRO-Mk3-6-0	1.875 × 1.875L18 (T63)	CSIRO-QCCCE	Yes / No	Rotstayn et al. (2012)
*GFDL-CM3	2.5 × 2L48 (C48)	GFDL	Yes / No	Delworth et al. (2006)
INM-CM4	2 × 1.5L21	INM	Yes / No	Volodin et al. (2010)
IPSL-CM5A-LR	3.75 × 1.89L39	IPSL	Yes / No	Hourdin et al. (2013)
IPSL-CM5A-MR	2.5 × 1.2587L39	IPSL	Yes / No	Hourdin et al. (2013)
IPSL-CM5B-LR	3.75 × 1.9L39	IPSL	Yes / No	Hourdin et al. (2013)
*MRI-CGCM3	1.125 × 1.125L48 (T159)	MRI	Yes / No	Yukimoto et al. (2012)
CMCC-CM	0.75 × 0.75L31 (T159)	CMCC	Yes / N/A	Scoccimarro et al. (2011)
FGOALS-g2	2.8125 × 2.8125L26	LASG-CESS	Yes / N/A	Li et al. (2013)
*HadGEM2-AO	1.875 × 1.24L60	MOHC	Yes / N/A	Martin et al. (2011)
*ACCESS1-0	1.875 × 1.25L38 (N96)	CSIRO-BOM	Yes / Yes	Bi et al. (2013)
*ACCESS1-3	1.875 × 1.25L38	CSIRO-BOM	Yes / Yes	Bi et al. (2013)
*HadGEM2-CC	1.875 × 1.24L60 (N96)	MOHC	Yes / Yes	Martin et al. (2011)
*HadGEM2-ES	1.875 × 1.24L38 (N96)	MOHC	Yes / Yes	Bellouin et al. (2011)
*MIROC5	1.40625 × 1.40625L40 (T85)	MIROC	Yes / Yes	Watanabe et al. (2010)
*MIROC-ESM	2.8125 × 2.8125L80 (T42)	MIROC	Yes / Yes	Watanabe et al. (2011)
*NorESM1-M	2.5 × 1.9L26 (F19)	NCC	Yes / Yes	Bentsen et al. (2013)
*NorESM1-ME	2.5 × 1.9L26	NCC	Yes / Yes	Bentsen et al. (2013)

Tab. 1. The CMIP5 models used in this study

As shown in Table 1, the analysed CMIP5 models have different horizontal resolution, number of vertical levels in the atmosphere, and representation of the aerosol effects. It is worth underlying that some of these climate models share a common lineage and are not really independent of each other, either because they share a common dynamical core (in particular the same atmospheric model) or they are developed in the same centre.
In this work we have analysed the effect of the aersol representation in the models on the modelled precipitation. It is well known, in fact, that especially in the monsoon-dominated

regions, precipitation is influenced by aerosol particles that act in both direct and indirect ways as climate drivers.

The mean annual cycle of precipitation, averaged over the years 1901-2005 (2006-2100) for the historical (future) climate, is shown in Figure 1 for the Himalaya (a) and HKK (b) regions. Each grey line indicates the output of a single model member, the multi-model mean (MMM) is shown with the black solid line, while CRU and GPCC observations are shown with the pink and green lines, respectively. With respect to CRU, the CMIP5 MMM indicates an overestimation of the simulated precipitation all over the year in both the HKK and Himalayan regions, a positive bias which is commonly found in the precipitation simulated by the state-of-the-art GCMs over high-elevated terrains. The same model bias is found with respect to GPCC data, except for July and August precipitation in the HKK region. In both regions, the model spread relative to the multi-model mean is large, indicating that the models do not converge in their representation of the historical precipitation annual cycle. Despite this, all models reproduce one-modal precipitation annual cycles in the Himalayan region, even if the various distributions are differently wide and have different amplitudes, while the model disagreement is much more serious in the HKK region, where annual cycles with very different characteristics are simulated (Palazzi et al., 2014).

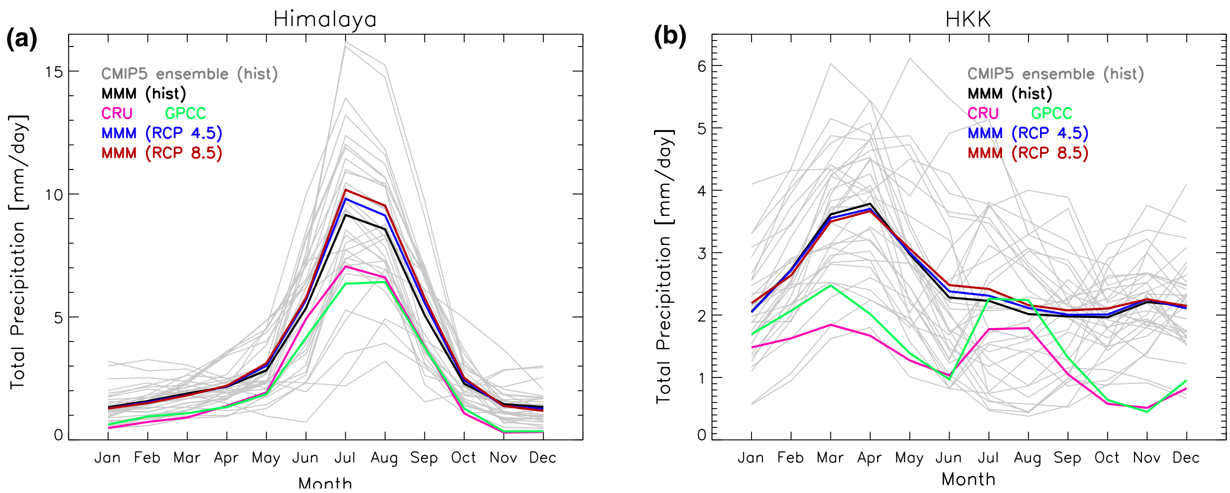

Fig. 1. Mean annual cycle of precipitation in the Himalaya (a) and HKK (b), obtained as a multi-annual average over the years 1901– 2005 (historical period) for each CMIP5 model (grey lines) and for their multi-model mean (MMM, black line). The solid blue and red lines represent the mean annual cycle of precipitation over the years 2006–2100 in the RCP 4.5 and the RCP 8.5 future scenarios, respectively, for the CMIP5 MMM

A hierarchical clustering analysis, using a standard Euclidean distance as a distance metric, has been applied to group the various models based on their output in terms of precipitation annual cycle in the HKK and Himalaya region, so assuming no a priori knowledge about the features of any model. Using the simplest rule of thumb to set the number of clusters, the procedure allowed to determine four model clusters in both regions and to identify the better performing models in the the HKK and Himalaya domains (not shown gere, see Palazzi et al., 2014).

An important outcome of the performed cluster analysis is that no feature of the better-performing models in the Himalaya or in the HKK region has clearly emerged as one playing a pivotal role for providing the best results in terms of precipitation annual cycle in the two regions. To better explore this issue, a further imposed “a priori” clustering was applied, based on the known characteristics of the models. Figure 2 shows, for the Himalaya and for the HKK sub-region, the precipitation annual cycles simulated by the models (grey area) and by their MMM (black line), grouped using the following criteria: models that do not/do include the indirect effects of sulfate aerosols (panels a/b); models that do not/do include fully-interactive aerosols (c/d); models with low/high horizontal resolution along longitudes (e/f; the models with a resolution coarser than 1.40625° longitude have been considered low-reso- lution models); models with low/high vertical resolution (g/h; the models with less then 47 vertical levels have been classified as low vertical resolution models). The division of models into high/low vertical and horizontal resolutions was made arbitrarily.

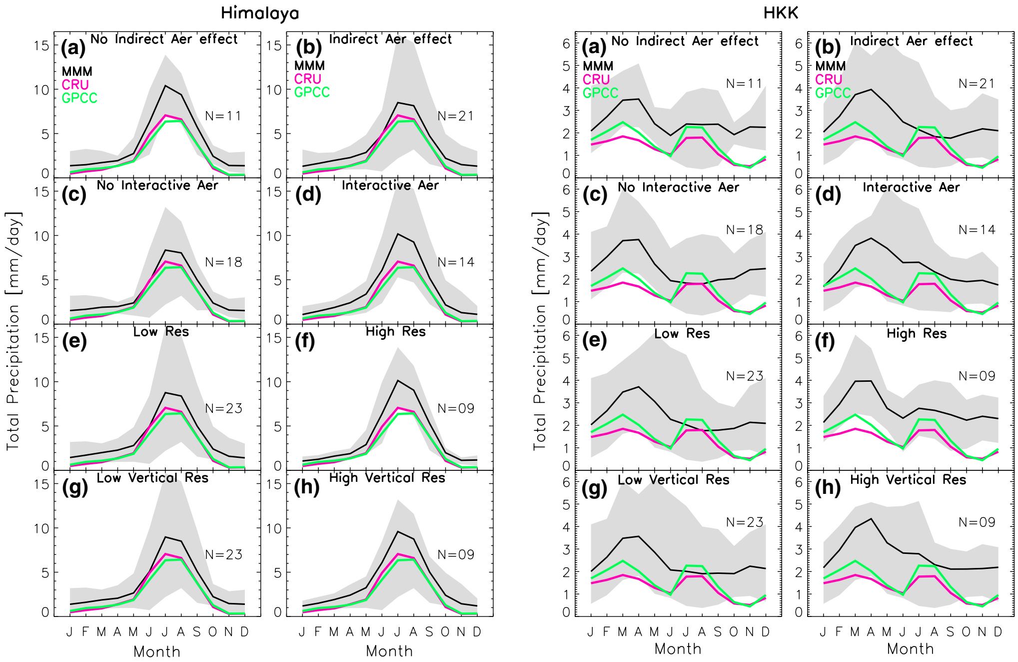

Fig. 2. Mean annual cycle of precipitation in the Himalaya (left panels) and in the HKK (right panels) simulated by all models which do not (a)/do (b) include the indirect effect of sulfate aerosols; have not (c)/have (d) fully-interactive aerosols; have low (e)/high (f) horizontal resolution; have low (g)/high (h) vertical resolution. The grey shaded areas indicate the variability range of the models; the MMM is shown with the black line while CRU and GPCC observations with pink and green lines, respectively. The number of models within each cluster is indicated in the plots.

Just focusing on aerosols, this further analysis shows that, in the Himalaya region, the models including the indirect effects of sulfate aerosols reproduce a precipitation annual cycle which is closer to the observations than the models incorporating the direct effect of sulfate aerosol only. The same is found for the models with prescribed aerosols with respect to those incorporating a fully-interactive aerosol. In the HKK sub-region, the best performing models are those which do not include the indirect effect of sulfate aerosols.

Reference paper:

PALAZZI E., VON HARDENBERG J., TERZAGO S., PROVENZALE A., (2014): Precipitation in the Karakoram-Himalaya: a CMIP5 view. *Climate Dynamics*, doi: 10.1007/s00382-014-2341-z.

D2.6.3e: Multi-secular historical climate simulation for the Mediterranean area and comparison with paleoclimatic proxy data, to obtain a climatological history of Italy in the last one thousand years

Lead Author: Elisa Palazzi
CNR-ISAC Torino.

Contributors: J. von Hardenberg
CNR-ISAC, Torino
A. Cuccu
University of Torino

The Planet Simulator (PlaSim) is an Earth System Model of Intermediate Complexity (EMIC) that was developed at the Meteorological Institute of the University of Hamburg and can be used to run climate and paleoclimate simulations for time scales up to 10 thousand years, due to its medium complexity and associated less intensive computing requirements.

Compared to other state-of-the-art EMICs (Claussen, 2002), PlaSim has a more complex atmospheric model (the Portable University Model of the Atmosphere, PUMA) based on the moist primitive equations conserving momentum, mass, energy and moisture and including, as in the most comprehensive general circulation models (GCMs), all atmospheric processes, but with the limitation of less sophisticated parameterizations (Fraedrich et al., 2005).

The atmospheric model in PlaSim can be coupled to different ocean models besides using climatological sea surface temperatures (SST). These ocean models can be a mixed-layer ocean or the large-scale geostrophic ocean (LSG, Maier-Reimer et al., 1993). Besides the atmospheric and oceanic parts, a land surface model with biosphere and a module representing sea ice can also be included. A complete description of how the coupling between the various components is realized can be found in the PlaSim User Guide (http://www.mi.uni-hamburg.de/fileadmin/files/forschung/theomet/planet_simulator/downloads/PS_UsersGuide.pdf).

The first objective of the research performed in this Pilot Study during the reference period was to test the different components of the PlaSim model and their coupling, and validate the PlaSim outputs against the EC-Earth global climate model outputs, in order to identify the model configuration to be used for further investigations. EC-Earth is one of the state-of-the-art GCMs participating in the Coupled Model Intercomaprison Project phase 5 (CMIP5) effort of the IPCC. Figures 1 and 2 show, respectively, the temperature and precipitation climatologies obtained with PlaSim, in which the atmospheric module, PUMA, has been coupled with (a) the Mixed Layer ocean module, (b) the LSG dynamical ocean module, and (c) the LSG + sea ice dynamical modules. Panels e), f), and g) of both figures show the difference between PlaSim and EC-Earth, in order to highlight the PlaSim performances with respect to the reference EC-Earth model.

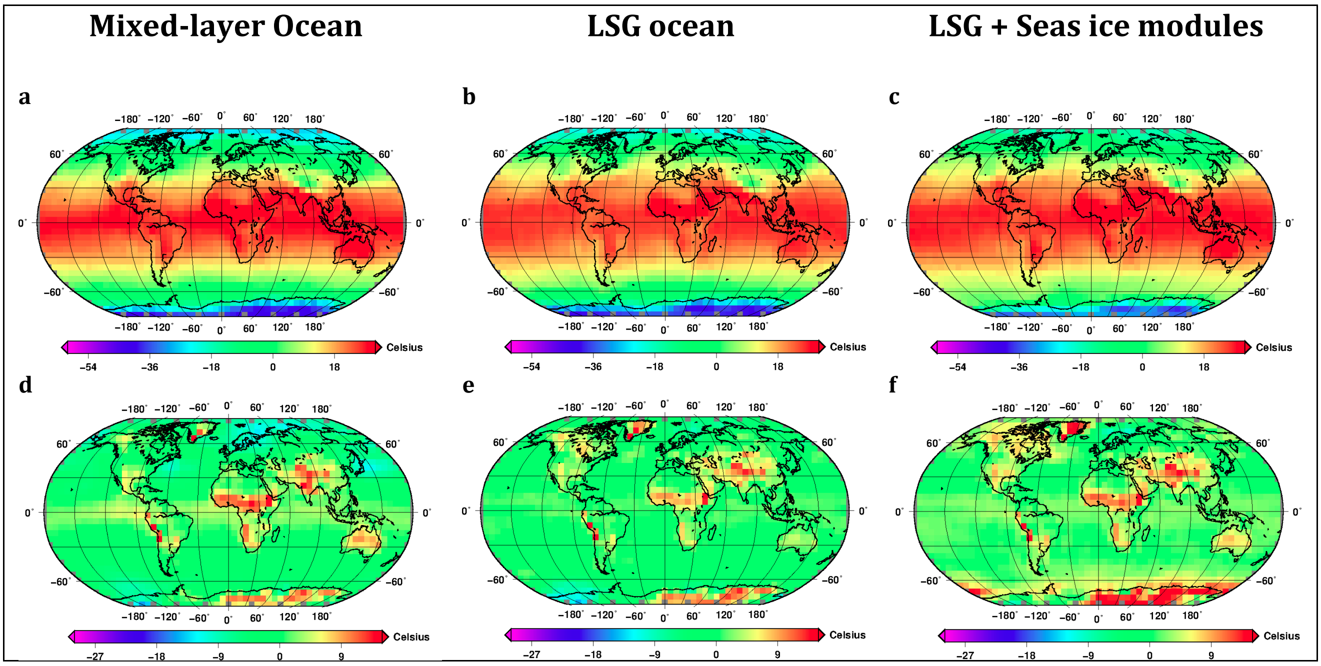

Fig. 1. Temperature climatology obtained with PlaSim, coupling PUMA with (a) the Mixed Layer ocean module, (b) the LSG dynamical ocean module, and (c) the LSG + sea ice dynamical modules. Panels e), f), and g) show the difference between PlaSim and EC-Earth outputs.

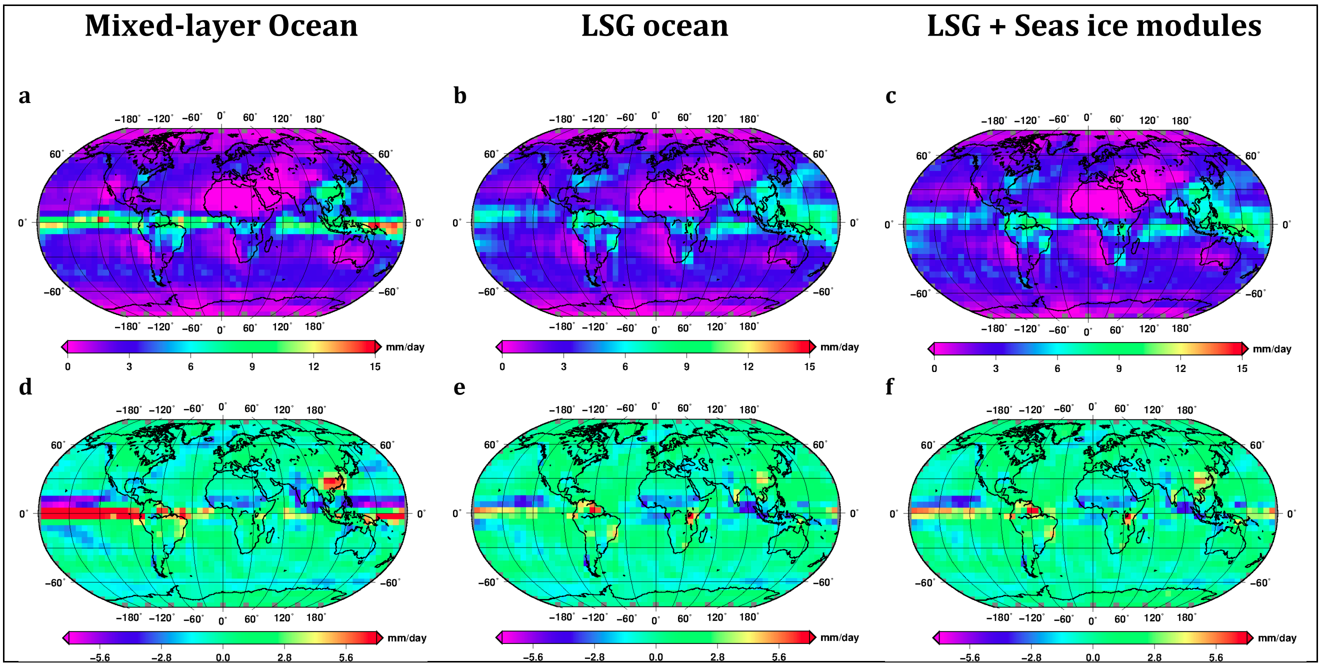

Fig. 2. The same as Figure 1 but for precipitation.

Given the outcomes of the previous analysis, in the first paleoclimate experiments performed with PlaSim we have considered the coupling of the atmospheric component, PUMA, with the dynamical ocean (LSG) and sea ice modules. First of all, we have studied the sensitivity of this coupled system to changes in the solar constant, by increasing or decreasing it up to the 10% of the actual value. For each new solar constant value we have performed perennial simulations up to 2000 years long, in order to allow the system to reach the equilibrium. Figure 3 schematically illustrates the procedure we have followed to perform these simulations.

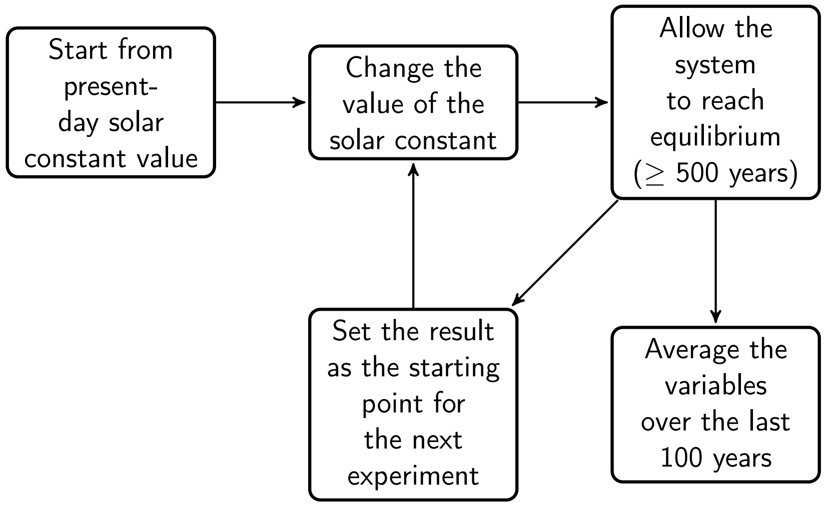

Fig. 3. Schematic of the procedure followed in the PlaSim simulations with varying solar constant values.

Results of these simualtions are shown in Figure 3 for the sea ice extent (top) and the temperature (bottom) variables; the red (green) line indicates the simulation branch in which the solar constant has been increased (decreased). As suggested by the figure, we found that, as in the simpler Energy Balance Models (EBMs), a snowball-earth solution and a hysteresis cycle is reproduced also by PlaSim simulations.

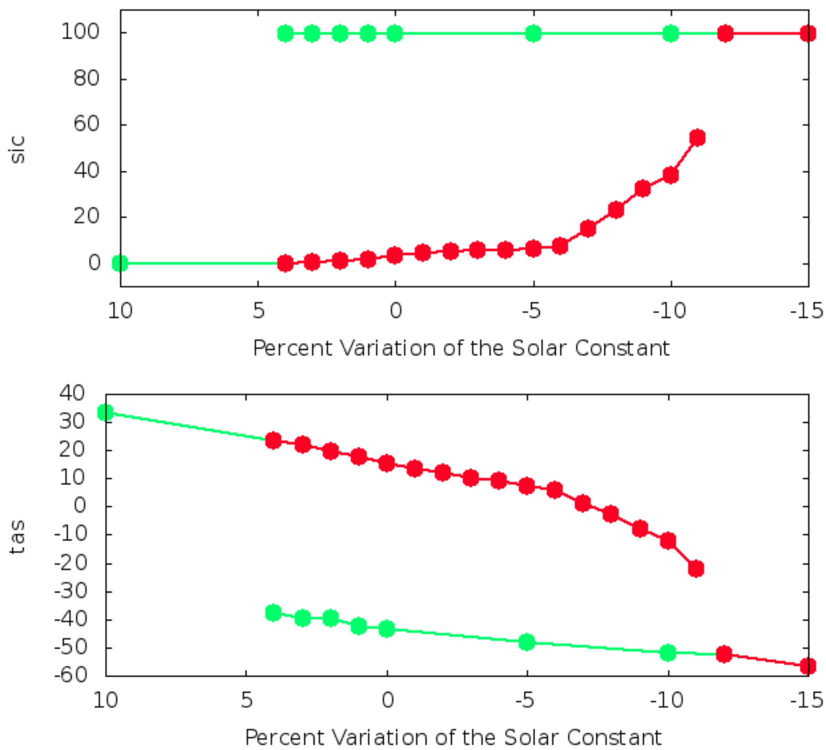

Fig. 4. Effect of solar radiation changes on the climate of the Earth (sea ice concentration above and temperature below) as seen by the PlaSim model.

For completeness, we show in Figure 5 the snowball Earth temperature and precipitation climatology.

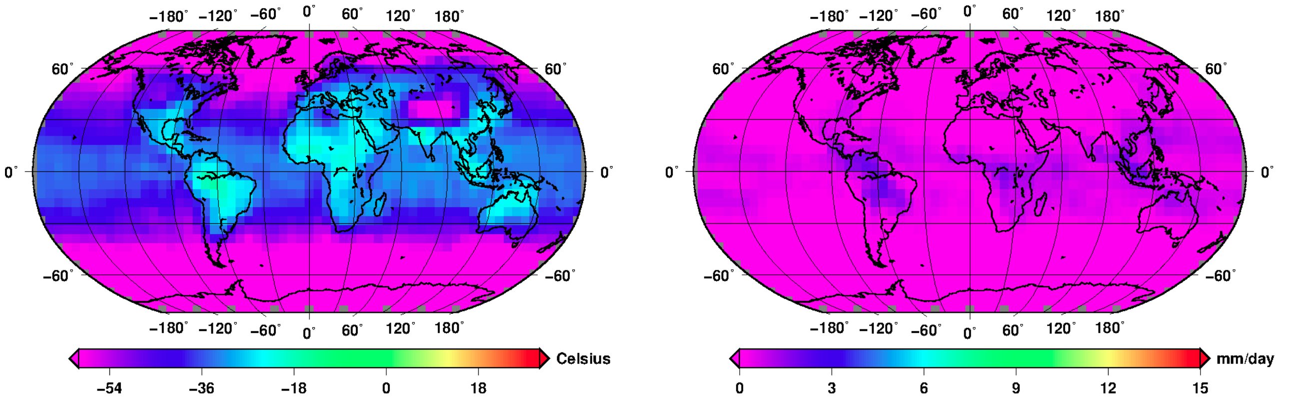

Fig. 4. Snowball Earth temperature and precipitation climatology.

Bibliography

CLAUSSEN M., L. A. MYSAK, WEAVER A. J., CRUCIFIX M., FICHEFET T., LOUTRE M.-F., WEBER S. L., ALCAMO J.,. ALEXEEV V. A, BERGER A., CALOV R., GANOPOLSKI A., GOOSE H., LOHMANN G., LUNKEIT F., MOKHOV I. I., PETOUKHOV V., STONE P., WANG Z., (2002): Earth system models of intermediate complexity: closing the gap in the spectrum of climate system models. *Climate Dyn.* 18, 579–586.

MAIER-REIMER E., MIKOLAJEWICZ U., and HASSELMANN K., (1993): Mean circulation of the Hamburg LSG OGCM and its sensitivity to the thermohaline surface forcing. *J. Phys. Oceanogr.,* 23, 731–757.

FRAEDRICH K., KIRK E., LUKSCH U., and LUNKEIT F., (2005): The Portable University Model of the Atmosphere (PUMA): Storm track dynamics and low frequency variability. *Meteorol. Zeitschrift,* 14, 735-745.

HAZELEGER W., WANG X., SEVERIJNS C., STEFAˇNESCU S., BINTANJA R., STERL A., WYSER K., SEMMLER T., YANG S., VAN DEN HURK B., VAN NOIJE T., VAN DER LINDEN E., VAN DER WIEL K., (2012): Ec-earth v2.2: Description and validation of a new seamless earth system prediction model. *Clim Dyn* 39, 2611–2629, DOI 10.1007/s00382-011-1228-5.

2.6f (Special Project P2): NextSnow - Measurement and analysis of precipitation in high-elevation regions

Lead Author: Vincenzo Levizzani (CNR-ISAC Bologna).

Contributors: S. Laviola, E. Cattani (CNR-ISAC); U. Morra Di Cella, E. Cremonese (ARPA-VdA); R. Rudari, S. Gabellani (CIMA Foundation); P. Claps, F. Laio, P. Allamano, A. Libertino (Politecnico di Torino – DIATI); S. Ferraris, D. Canone, M. Previati (Politecnico e Università di Torino – DIST); C. Cassardo, S. Ferrarese (Università di Torino – Dip. Fisica); S. Fratianni, F. Acquaotta, D. Garzena, L. Perotti (Università di Torino – Dip. Scienze della Terra).

2.6g (Special Project P3): Database for reconstructing the spatial-temporal evolution of the Glacial Resource in the Italian ALPs over the last 100 years in the Framework of the NextData Project (DATAGRALP)

Lead Author: Marta Chiarle (CNR-IRPI, Torino).

Contributors: C. Baroni, A. Carton, M. Chiarle, M. Giardino, G.Mortara, G. Nigrelli, L. Perotti, M. C. Salvatore (CNR-IRPI, CGI).

D2.6h (Special Project P7): High Resolution Climate Information for Mountain Areas (HR- CIMA)

Author: Michele Brunetti
CNR-ISAC, Bologna

Contributors: A. Bertolini, M.Brunetti, C. Simolo
CNR-ISAC, Bologna
M. Maugeri
Dipartimento di Fisica – Università di Milano

Inventory of monthly temperature and precipitation data available in digital form for the Italian Alpine area and surroundings.

1. Aim of the Deliverable

The aim of this Deliverable was to investigate how much the data availability (monthly temperature and precipitation) can be improved with respect to the present state of the art of the data archive used to assess and monitor present climate and its variability as far as the Italian Alpine region is concerned.

The inventory of monthly temperature and precipitation series available in digital form has been performed for some regions by establishing strict collaborative relationships with some very collaborative Regional Environmental Agencies (ARPAs) and for other regions by searching for official data freely available on the web.

Data inventory has been concentrated on Northern Italy regions (Valle d'Aosta, Piedmont, Liguria, Lombardy, Emilia-Romagna, Trentino Alto-Adige, Veneto and Friuli Venezia Giulia) and Switzerland.

2. State of the art

The present state of the art can be summarized in two kind of data sets: i) one consisting of both short temporal series and climate normal (i.e. climatologies) referred to a standard reference period, necessary to reconstruct the high resolution normal values of temperature and precipitation over the Italian Alpine area (see Task 3 and it Deliverables 3.1 and 3.2), but not useful to evaluate climate changes and variability; ii) the other consisting of long temporal series (more than 30 year long and hopefully at least half century) quality checked and homogenized, necessary to assess how climate changed in the past and useful to reconstruct the temporal component of the data sets for the three case studies (Task 4 and its Deliverable 4.1).

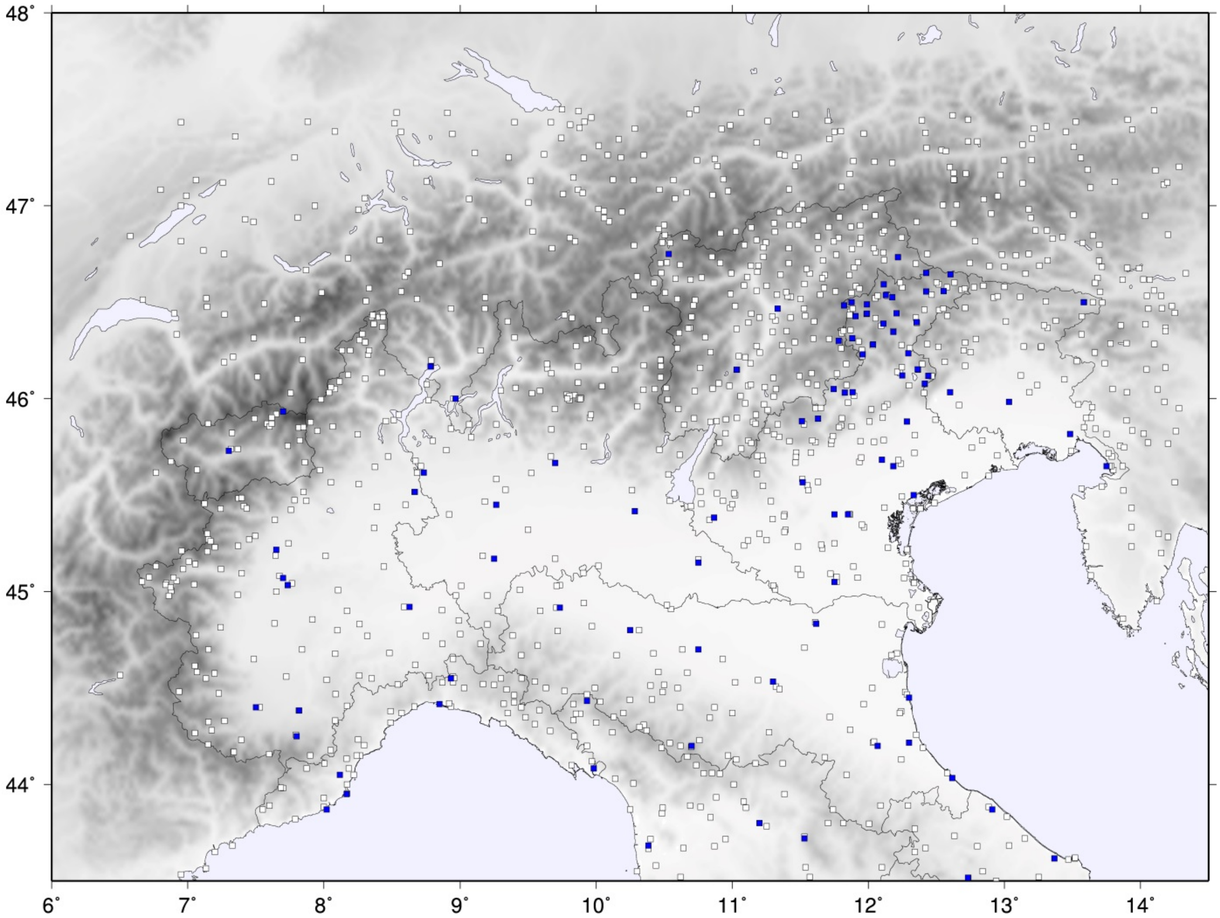

Fig. 1. Temperature series available before the Special Project HR-CIMA. White squares are stations with only climate normal available; blue squares refer to stations with long temporal series are available in already homogenized form.

2.1 Temperature

For temperature, a data set of climate normal (CLINO) referred to the 1961-1990 reference period was realized for Italy to produce a first guess of mean temperature climatology at 30 arc-second of spatial resolution (Brunetti et al., 2014) and associated confidence interval.
This data set consists of 1608 mean temperature CLINOs (for part of them also minimum and maximum values are available), but only 1127 of these station data are located at latitude north of 43° (more or less the area of Italy focus of the present Special Project) and is presented in figure 1 (white squares).
Brunetti et al. (2014) highlighted both the good performances of the presented interpolation procedure, but also the weaknesses of the present data set, for the Alpine area in particular, where the confidence interval is quite large. This is partly due to the low number of station available for high elevation sites: only 379 of these stations are located at an elevation above 1000 m, and only 174 above 1500 m.
As far as long temporal series are concerned, the present state of the art consists of the blue squares shown in figure 1, comprising the homogenized data sets presented in Brunetti et al. (2006) updated with the data presented in Simolo et al. (2010) and some additional stations selected for the realization and maintenance of the ISAC-CNR Climate Monitoring Bulletins (www.isac.cnr.it/climstor/climate_news.html).

2.2 Precipitation

As far precipitation is concerned, the state of the art consists in a rough data set of not quality checked precipitation series. The series length is very heterogeneous: part of them can be exploited only to extract CLINOs over a standard reference period, others can be useful, after homogenization, for a fruitful temporal analysis. All together these data series consists of 3731 stations all over Italy, 2115 of which are located north of 43° (white squares in figure 2). Beside this rough data set, there is a core data set of secular series that have been homogenized by Brunetti et al. (2006), 62 of them are located in Northern Italy together with a set of 75 precipitation series homogenized by Brugnara et al (2010) and few other Air Force series a total of 169 station series were available before the starting of the present Project. All these series are shown in figure 2 (blue squares). Only 60 of these stations are located at an elevation above 1000 m and only 17 above 1500 m.

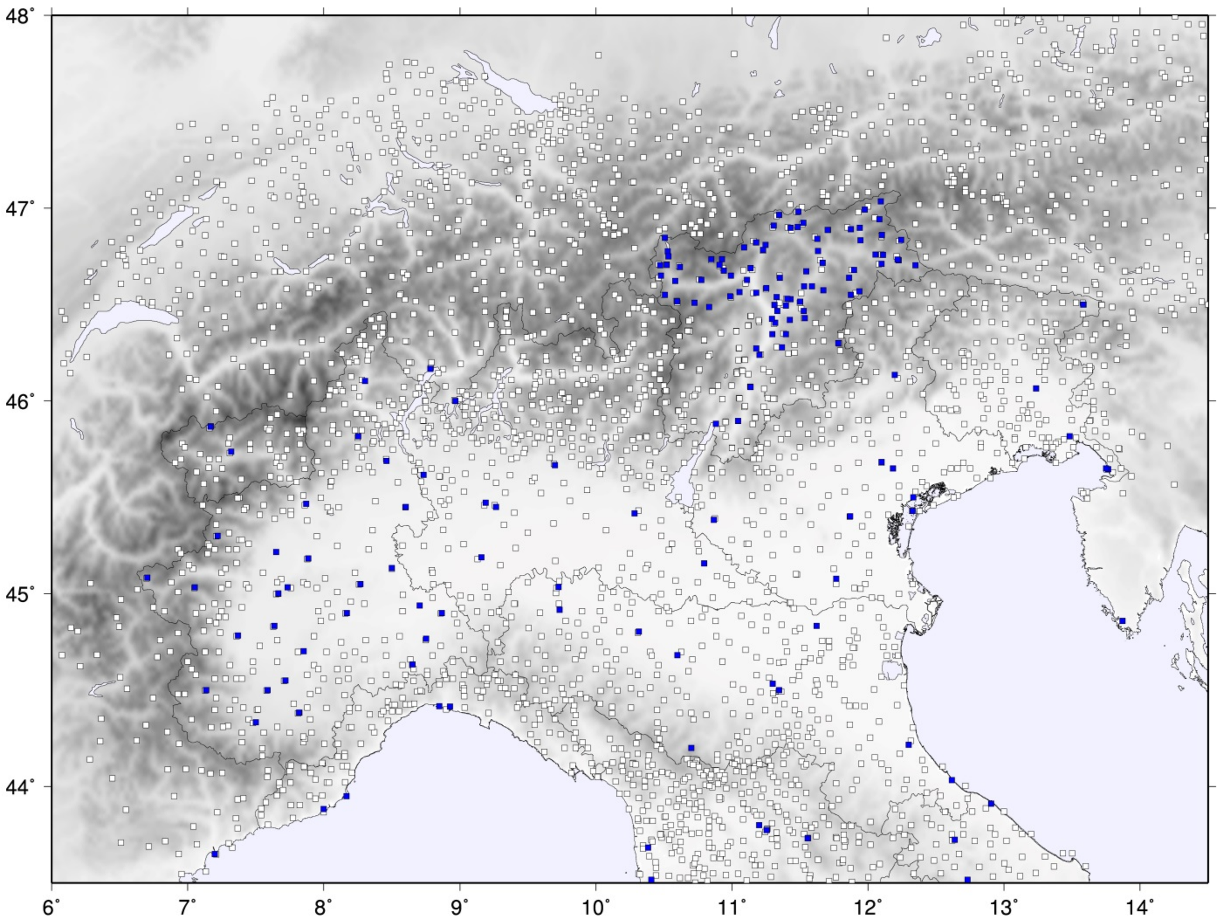

Fig. 2. Same as figure 1, but for precipitation.

3. Inventory of potentially available data

The data shown in figures 1 and 2 are only a fraction of the heritage of digital data available for the study area.

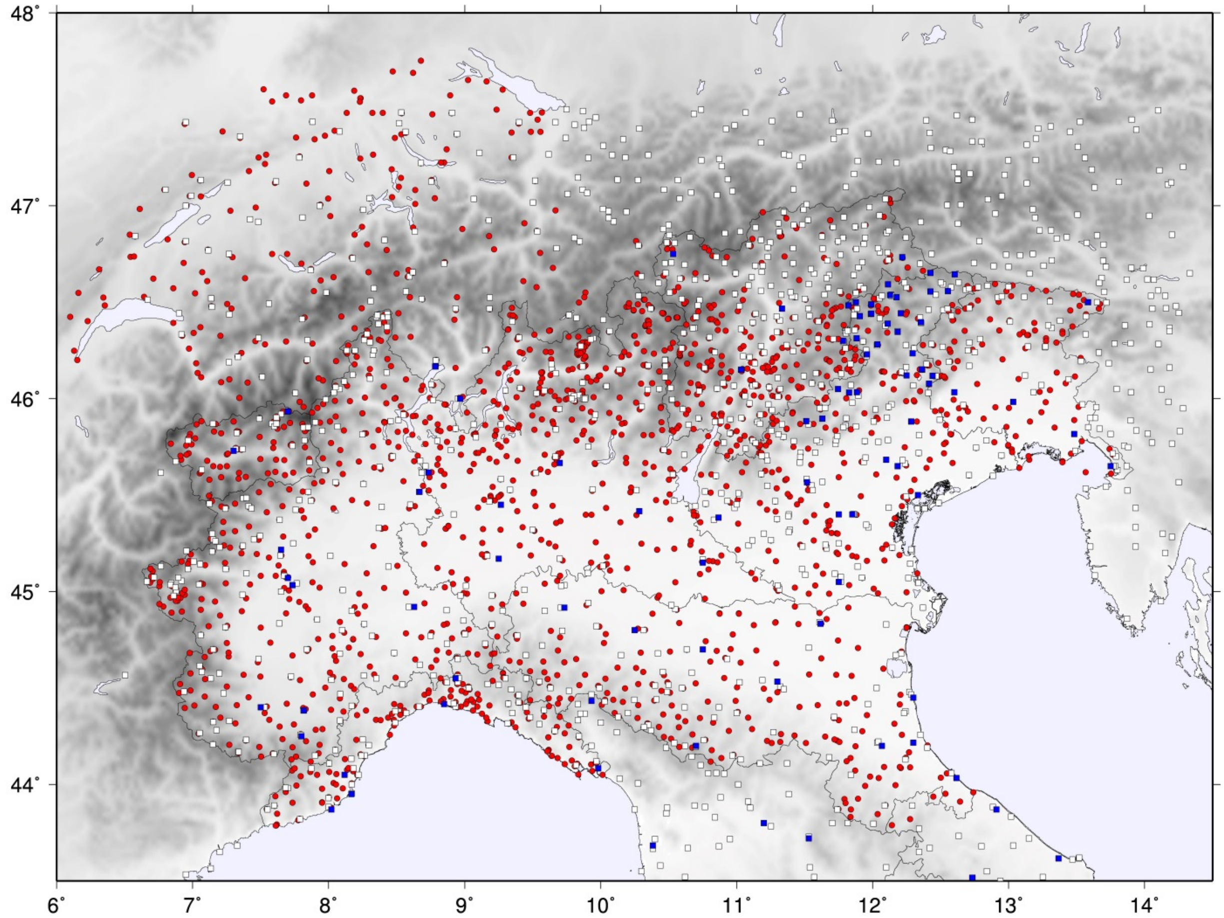

Fig. 3. Potential improvement in temperature data availability. White and blue squares as in figure 1; red dots refer to the new stations identified by the inventory activity.

From a detailed but not exhaustive (we concentrated our research at a regional scale, without exploiting the existing sub-region data sets) inspection of the WMO-standard networks available in Northern Italy regions (Valle d'Aosta, Piedmont, Liguria, Lombardy, Emilia-Romagna, Trentino Alto-Adige, Veneto and Friuli Venezia Giulia) and Switzerland, we selected 2910 precipitation stations and 1930 temperature stations (for some regions the series with less than 10 years of data were already excluded).

All these series potentially (all those with less than 10 years of available data will be discarded) increase the stations' availability as shown in figures 3 and 4 for temperature and precipitation respectively.

361 (637) and 316 (650) of the new stations (for temperature and precipitation respectively) are located above 1500 m (1000 m) (there are other 76 and 152 stations, for temperature and precipitation respectively, for which the elevation information was not available and must be recovered in some way).

To conclude, Italy has a great heritage of data that, if exploited all together, can provide a robust base to reconstruct the present climate information at a very local scale.

The present Project will provide an example of what can be done, in terms of spatial resolution and confidence level, if all the available data were put together into one single data set.

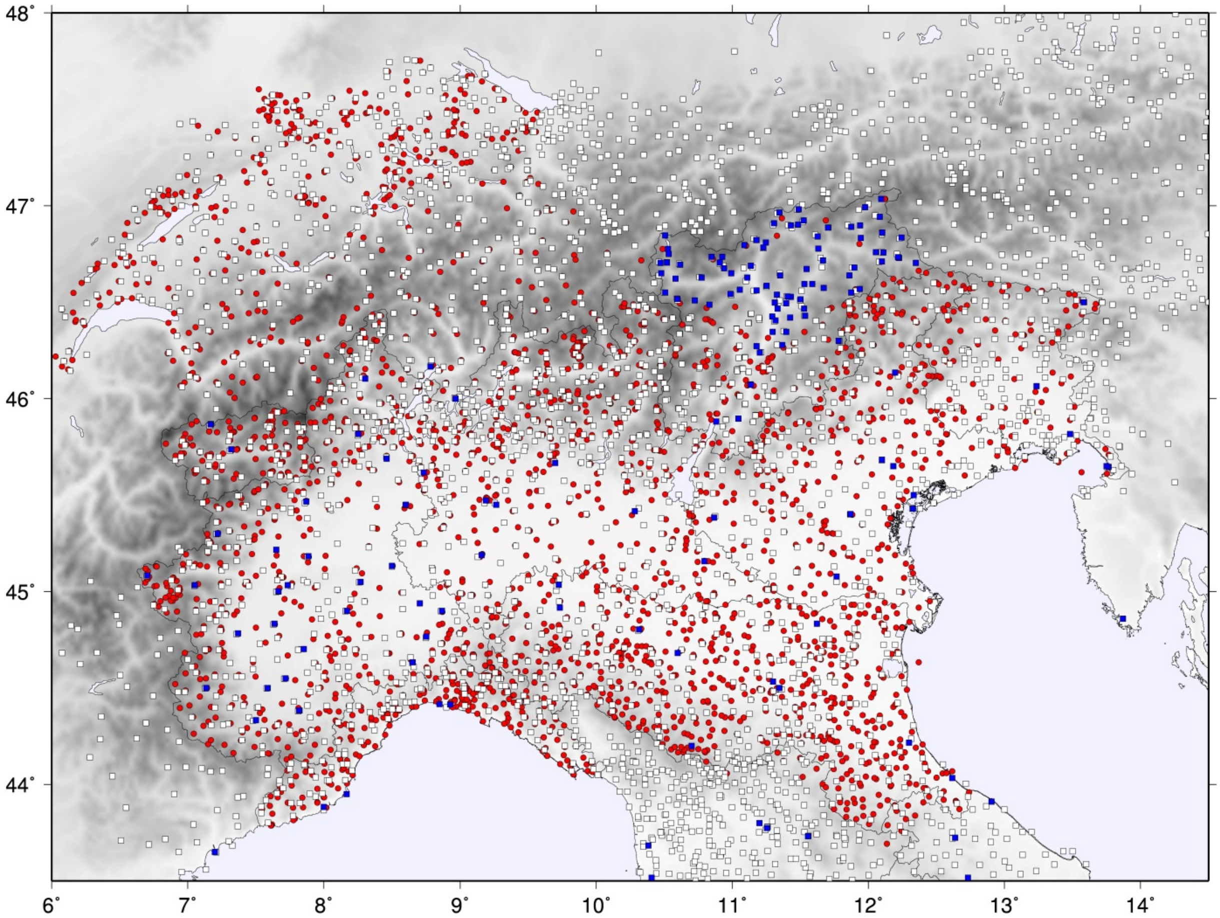

Fig. 4. As figure 3, but for precipitation

References:

BRUGNARA Y., BRUNETTI M., MAUGERI M., NANNI T., SIMOLO C., (2012): High-resolution analysis of daily precipitation trends in the central Alps over the last century. *International Journal of Climatology*, 32, 1406-1422, DOI: 10.1002/joc.2363.

BRUNETTI M., MAUGERI M., MONTI F., NANNI T., (2006): Temperature and precipitation variability in Italy in the last two centuries from homogenized instrumental time series. *International Journal of Climatology* (ISSN 0899-8418), 26, 345-381.

BRUNETTI M., MAUGERI M., NANNI T., SIMOLO C., SPINONI J., (2014): High-resolution temperature climatology for Italy: interpolation method intercomparison. *International Journal of Climatology*, 34, 1278-1296.

SIMOLO C., BRUNETTI M., MAUGERI M., NANNI T., SPERANZA A., (2010): Understanding climate change-induced variations in daily temperature distributions over Italy. *Journal of Geophysical Research - Atmosphere* (ISSN 0148-0227), 115, D22110, doi:10.1029/2010JD014088.

D2.6j: HAMMER Special Project

HAMMER - RelationsHips between meteo-climAtic paraMeters and ground surface deforMation time sEries in mountain enviRonments

Lead Authors: F. Ardizzone, M. Cignetti, A. Manconi
CNR-IRPI, Perugia, Torino

Contributors:
D. Giordan, P. Allasia
CNR-IRPI, Torino

M. Manunta
CNR-IREA, Napoli

Introduction

HAMMER aims to reconstruct ground surface deformation time series in test areas located in mountain environments, and to analyse the correlation between the ground deformation and meteo-climatic time series. HAMMER also aims to implement data and results in digital archives compatible with the NextData Project archives. The Project focuses on the following study areas: (i) Italian Western Alps, (ii) Apennines, (iii) Pyrenees, and (iv) Atacama desert, Andes (Figure 1).

This document reports the activities developed during the period from January to December 2014 in the framework of HAMMER Project, as required by the Project proposal. The Project required:

1. Collection and organization of surface and sub-surface deformation provided by *in-situ* monitoring systems available for test sites in the Alps and the Apennines.
2. Collection and organization of ground deformation DInSAR time series already processed for test sites in the Apennines, the Andes and Pyrenees.
3. Systematic search of the surface deformation information available through the *Piano Straordinario di Telerilevamento Ambientale* (http://www.pcn.minambiente.it/viewer/) for selected study areas in the Alps and the Apennines.
4. Systematic search of the surface deformation information available through a literature review.
5. Collection of meteorological/climate time series for relevant meteorological stations in the study areas.

The report is organize as follows:

- Section 2 illustrates the state of art of the Project.
- Section 3 describes the test sites and the data collected in framework of the Project first year.
- Section 4, describes the new SAR data that has been produced with ESA's G-POD (http://gpod.eo.esa.int/) service.
- Section 5 is dedicated to the description of the FTP structure, temporarily used to store and transfer data and metadata.
- Section 6 includes the description of the analysis of the scientific and technical literature carried out to determine where quantitative surface and sub-surface information on ground deformations in landslide areas is available, and for which periods was made.

- Section 7 reports the cited literature.

State of art

The analysis of surface movements aims to define the geomorphological evolution of single or multiple landslides. The short-term analysis of surface movement is obtained through quantitative or semi-quantitative analyses of three-dimensional topographic data and high accuracy measurements obtained exploiting different monitoring techniques (Giordan et al., 2013). The combined analysis of ground displacement time series and meteorological/climatic measurements may contribute to understand the response of unstable slopes to short-term meteorological triggers and long-term climatic forcing (Lollino et al., 2006; Burda et al., 2013; Crosta et al., 2013).

In the last decades several *in situ* monitoring techniques were considered, including Total Station, GPS receivers, Terrestrial LiDAR, Ground Based Radars, extensometers and inclinometers. These tools are essential to provide ground deformation time series with very high temporal sampling, allowing for the reconstruction of the evolution of the single landslide phenomena over time. The possibility of obtaining long time series of deformation relevant to several landslides in different physiographic and climatic region may open the possibility of understand the complex, and largely unknown, relationships between climate and its variations, and study the initiation and development of the deep-stated landslides (Calò et al., 2013).

In the period from March to August the work has been focused on four study areas located in the Alps and Apennines territory, where information about time series of ground deformation has been collected. Most of the ground deformation data has been obtained from previous internal studies prepared by CNR-IRPI Torino (http://gmg.irpi.cnr.it) and by the CNR-IRPI Perugia (http://geomorphology.irpi.cnr.it/) and also from several publications (Calò et al., 2014; Lollino et al., 2006). In the period from August to December, the work has been focused on the study areas in the Alps, in the Pyrenees in order to collect all the available SAR data. Furthermore, new SAR mean velocity maps and time series for two specific sectors have been generated using the ESA's G-POD (http://gpod.eo.esa.int/) service.

1 GROUND DEFORMATION TIME SERIES and MEteo-climatic parameter collection

During the first years the work has been focused on the European test sites. The Italian sites are located in the Alps territory, Gardiola and Grange Orgiera landslides, and two test sites in the Apennines territory, Montalto di Cosola and Ivanciich landslides. Table 1 and Figure 1 show the location of the test sites. The Spanish test area corresponds to Tena Valley (Central Pyrenees) where several landslides affect the territory (Figure 1).

Tab. 1. HAMMER test sites distributed in the Alps and Apennines territory, associated to their geographic coordinates.

Test Site	Location	Coordinates
GARDIOLA	Germanasca Valley – Prali, Piemonte, Northern Italy	44°55'29N - 7°3'52E
GRANGE ORGIERA	Varaita Valley – Sampeyre, Piemonte, Northern Italy	44°36'21N - 7°8'2E
MONTALDO di COSOLA	Cabella Ligure municipality, Alessandria, Piemonte, Northern Italy	44°40'4N - 9°10'43E
IVANCICH	Assisi municipality, Perugia, Umbria, Central Italy	43°4'8N - 12°37'51E

Fig. 1. View on Google Earth of the HAMMER Test Sites.

For each Italian test area, *in-situ* monitoring techniques were considered, including Total Station and inclinometers. Meteorological data were also gathered from meteorological station close to each test site. The collection of available SAR data was realized for Ivancich landslide and El Portalet landslide (Figure 1).

1.1 Gardiola Test Site

The Gardiola landslide is a complex lanslide in Salza di Pinerolo, in the central part of the Germanasca Valley (Piemonte, Italy). The landslide was reactivated during the flood event occurred on 14-16 October 2000. A temporary *in-situ* monitoring network, consisting in several optical targets located in the most active sector of the landslide, has been installed since October 2000. Subsequently, this network has become a permanent monitoring network since 2004, consisting in a topographic network with a Robotic Total Station (LEICA 2003 with Automatic Target Recognition ATR), surveying 23 optical targets, three of which located outside landslide on the stable ground. The topographic network is associated to four extensometers, an inclinometer, a piezometer and a GPS monitoring network.

For this test site, we collected ground deformation time series (GMG Group - CNR Torino Internal Data) relevant to the permanent topographic monitoring network. The time series provide x, y, z local coordinates, and Δx, Δy, Δz, and total displacement Δtot data of 19 prisms target.

To describe the landslide, from a geomorphological point of view, and to represent the location of the monitoring instruments, point, linear and polygonal shape files were created (Figure 2), using the open source software QGIS 2.2 Valmiera (http://www.qgis.org/it/site/).

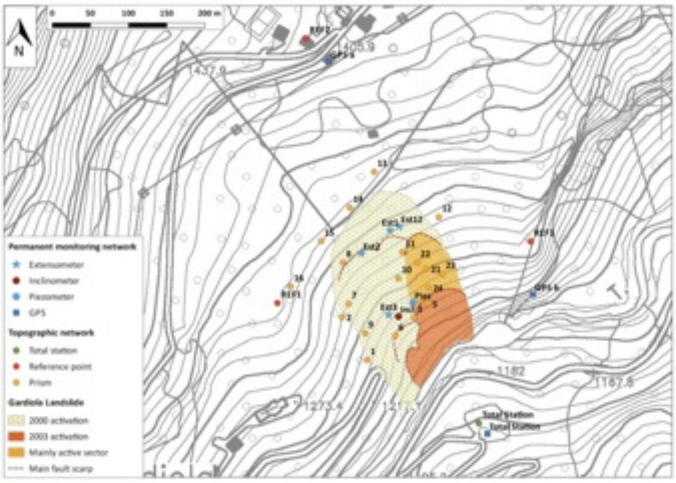

Fig. 2. Permanent monitoring network of Gardiola landslide.

Meteorological data were collected at the Prali Villa Meteorological Station located about 3 km south-southwest of Gardiola landslide in the Prali Villa municipality (Pellice Valley, Piemonte, Italy). The Arpa Piemonte meteorological network (http://www.regione.piemonte.it/ambiente/aria/rilev/ariaday/annali/meteorologici) provided the data. The station sensors register: temperature (average, maximum and minimum), rainfall (24 hours) and snow (snow depth, snow cover) data. Daily and monthly rainfall data are delivered, including also high precipitation for the 1993 – 2013 time period.

1.2 Grange Orgiera Test Site

The Grange Orgiera landslide is a complex landslide located in Varaita Valley, at the Villar hamlet (Sampeyre, Cuneo, Piemonte, Italy). The landslide moved on July 2009, after later spring rainfall following intense snow precipitations occurred in the 2008-2009 winter. Since August 2009 the landslide was monitored with a topographic monitoring network made up of a total station, 6 prisms inside the landslide and 2 prisms outside the landslide, close to the landslide foot. The monitoring network included also a GPS system made up 8 benchmarks inside the landslide and 8 outside. In July 2010, 5 new prisms within the landslide body, near to the left frontal lobe of the landslide, have been installed.

For this test site we collected the ground deformation time series from topographic monitoring network (CNR-IRPI Torino, GMG group Internal Data). In particular, two time series from August 2009 to October 2009 and from July 2010 to September 2010 were collected. These time series provide x, y, z local coordinates, Δx, Δy, Δz, and total displacement Δtot data respectively for 8 prisms target for the 2009 monitoring campaign and for 13 prisms target for the 2010 monitoring campaign.

To describe the landslide, from a geomorphological point of view, and to represent the location of the monitoring instruments, point, linear and polygonal shape files were created (Figure 3), using the open source software QGIS 2.2 Valmiera (http://www.qgis.org/it/site/).

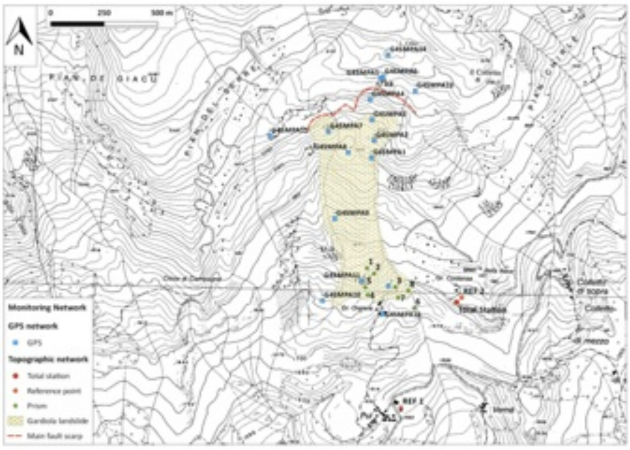

Fig. 3. Monitoring network of Grange Orgiera landslide.

Meteorological data were collected at Sampeyre/Capoluogo and Pian delle Baracche Meteorological Stations close to Grange Origera landslide. The first one is located in Sampeyre municipality (Varaita Valley, Piemonte, Italy), about 5 km east-southeast of Grange Orgiera landslide, and the second one is located in Pian delle Baracche (Sampeyre municipality, Varaita Valley, Piemonte, Italy), about 6 km south of Grange Orgiera landslide. The Arpa Piemonte meteorological network (http://www.regione.piemonte.it/ambiente/aria/rilev/ariaday/annali/meteorologici) provided the data. The station sensors register: temperature (average, maximum and minimum), rainfall (24 hours) and snow (snow depth, snow cover) data. Daily and monthly rainfall data are delivered, including also high precipitation for the 1988 – 2013 time period.

1.3 Montaldo di Cosola Test Site

The Montaldo di Cosola landslide is a complex slide located in Cabella Ligure municipality (Alessandria, Piemonte, Italy). The landslide reactivated in the flood event occurred in the 1993 autumn, and a monitoring network consisting of two inclinometers, an automated inclinometer system (AIS) and two piezometers was installed in the period from 2000 to 2001, furthermore three inclinometers, an automated inclinometer system (AIS) and six piezometers were installed in the period from 2002 to 2004. For this test site we collected ground deformation time series of the inclinometers data (Lollino et al. ,2006).

To describe the landslide, from a geomorphological point of view, and to represent the location of the monitoring instruments, point, linear and polygonal shape files were created (Figure 4), using the open source software QGIS 2.2 Valmiera (http://www.qgis.org/it/site/).

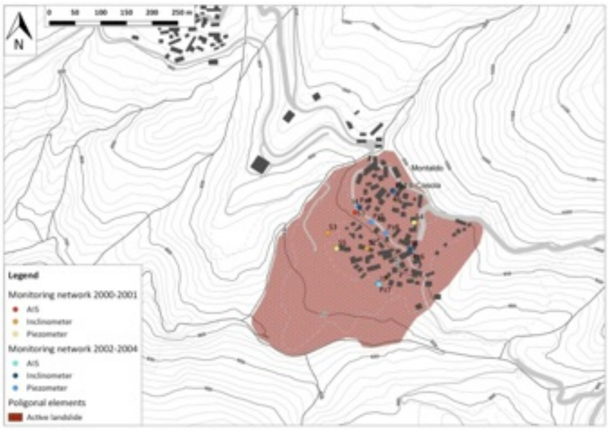

Fig. 4. Monitoring network of Montaldo di Cosola landslide.

Meteorological data were collected at the Cabella Ligure Meteorological Stations, about 7 km west to Montaldo di Cosola landslide in the Cabella Ligure municipality (Scrivia Valley, Piemonte, Italy). The Arpa Piemonte meteorological network (http://www.regione.piemonte.it/ambiente/aria/rilev/ariaday/annali/meteorologici) provided the data. The station sensors register: temperature (average, maximum and minimum) and rainfall (24 hours) data. Daily and monthly rainfall data are delivered, including also high precipitation for the 2006 – 2013 time period.

1.4 Ivancich Test Site

The Ivancich landslide is a translational slide with a rotational component in the source area, located in the Assisi municipality (Perugia, Umbria, Central Italy). Several monitoring instruments were installed to monitor the landslide: (i) a monitoring network (1998), consisting of 12 inclinometers and 42 piezometers, (ii) an integrative monitoring network (2001), consisting of an inclinometer, six piezometers and six settlement gauges, and (iii) an additional integrative monitoring network (2002-2003), consisting of five inclinometers and 8 piezometers, and a GPS monitoring network with 14 benchmarks. For this test site ground deformation time series of four inclinometers (CNR Perugia Internal Data – Calò et al., 2014) were collected.

To describe the landslide, from a geomorphological point of view, and to represent the location of the monitoring instruments, point, linear and polygonal shape files were created (Figure 5), using the open source software QGIS 2.2 Valmiera (http://www.qgis.org/it/site/).

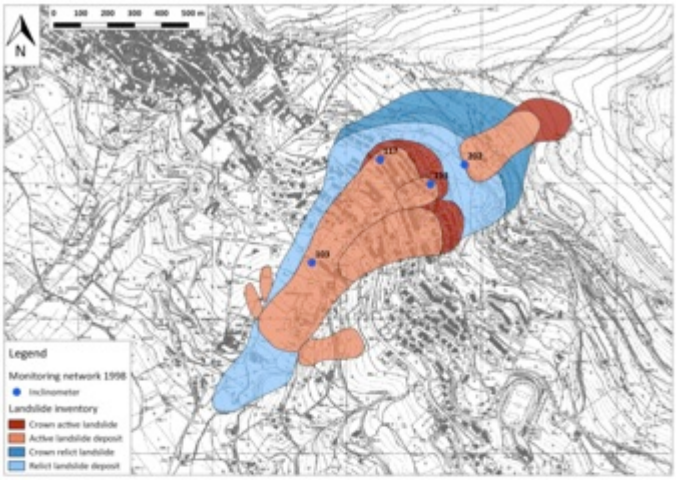

Fig. 5. Landslides inventory map and monitoring network of Ivancich. The shades of blue show ancient and relict landslides, and shades of red show recent landslides. The landslide crown areas (darker colours) are mapped separately from the landslide deposits (lighter colours) (Modified from Calò et al., 2014).

The meteorological data, for this test site were collected from Armenzano, Bastia Umbra and Cannara Meteorological Stations close to Ivancich Landslide. The Umbria Region meteorological network (http://www.idrografico.regione.umbria.it/annali/default.aspx) provided rainfall data. The time series consist of daily rainfalls for the 1988 – 2009 (Armenzano and Bastia Umbra stations) and 1988-2010 (Cannara station) time periods.

For Ivancich landslide available ground deformation, velocity maps and associated time series were acquired. The analyses of the surface deformation were obtained by applying the SBAS technique (Bernardino et al., 2002) to CosmoSky-MED, ERS-1/2 and ASAR-Envisat satellite images. The CosmoSky-MED satellite dataset, composed of 39 images in descending orbit spanning from December 2009 to February 2012, has been processed at low-resolution (30x30 m) and full-resolution scale (3x3 m); the ERS-1/2 and ENVISAT satellite dataset, composed of 87 images (36 ERS-1/2 and 51 ASAR-Envisat) in ascending orbit spanning from June 1995 to September 2010, has been processed at low-resolution scale (100x100 m), and also at full-resolution scale (5x20 m), while 130 images (91 ERS-1/2 and 39 ENVISAT), in descending orbit, spanning from April 1992 to November 2010, has been processed at full-resolution scale (5 m x 20 m). Figure 6 shows an example of the SBAS products; in particular the velocity map of the ERS-1/2 and ASAR-Envisat dataset, obtained with SBAS technique in descending orbit in full-resolution scale, is reported. Each point is associated to a ground deformation time series, for the observed period (1992 - 2010).

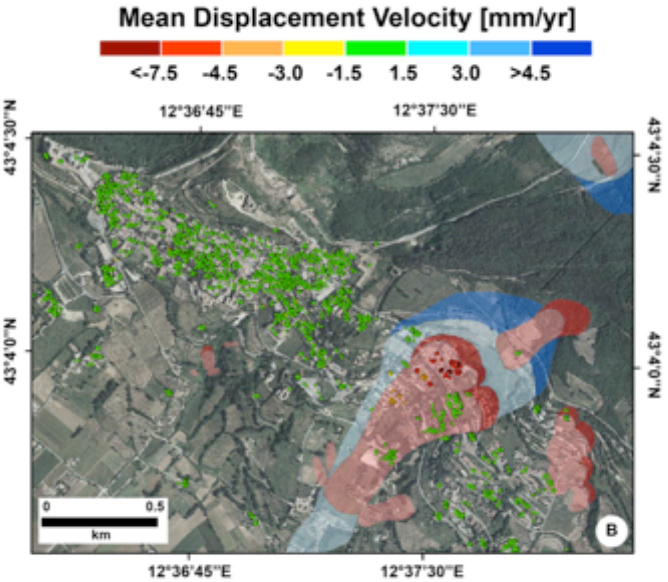

Fig. 6. Velocity map (cm/y) of ERS-1/2 and ENVISAT dataset, in descending orbit, for the period April 1992-November 2010, for the Ivancich landslide (Assisi, Umbria, Central Italy) (extracted by Calò et al., 2013).

1.5 Tena Valley test site

The Tena Valley is located in the upper part of Gállego River basin, in Central Spanish Pyrenees (Figure 1). Due the geological setting this area is affected by many landslide (Herrera et al., 2013). The climate is characterised by marked seasonability, with a considerable portion of the precipitation (> 30%) corresponds to snowfall that mostly occurs between December and March (Davalillo et al., 2014); furthermore the frost and snow coverage may melt rapidly in the late spring causing significant infiltration in a short period of time, with the consequent increase in the pore pressure of the slope materials, favouring landslide dynamic.

This territory has been investigated by geomorphological investigation, *in-situ* geotechnical investigation and recently by the DInSAR technology. ERS and Envisat data respectively for the period 1992-2000 and 2003-2010, in ascending and descending orbit were acquired by HAMMER Project. The datasets were available to us thanking the Framework Agreement between NextData Project and Terrafirma (GEMS ESRIN/Contract No. 4000109669/13/I-AM).

Meteorological data are available from the SAIH Ebro Confederación Hidrográfica del Ebro (Hispagua, Sistema Español de Informacíon sobre el Agua: http://hispagua.cedex.es/). The inspection of the website revealed that the data are subsequent to temporal interval covered by the ERS and Envisat data.

1.6 Salar de Atacama test site

The Salar de Atacama is located in the Atacama Desert (Chilean Andes), one of the most hyperarid deserts of the World. The Atacama Desert is a plateau located in South America, where a ground deformation (uplift) was revealed by space-borne InSAR analysis on salt lakes, named Salar (4000 – 5000 m a.s.l.). In that area several flanks of inactive volcanoes show gravitational processes, also considered in the test site. We focused to investigate the variation of the uplift trend and the variation of the velocity of the gravitational slopes interesting the flanks of the volcanoes using the space-borne ground deformation. For the purpose we have begun the processing of ERS-1/2 and ASAR-Envisat satellite images exploiting the ESA service named Grid Processing On-Demand G-POD (http://gpod.eo.esa.int/).

The meteorological data, available for this test site, are represented by the average, minimum and maximum temperature, and daily and monthly rainfall. The Direccĩõn General the Aguas, Ministero de Obras Pũblica, Gobierno de Chile provides the meteorological information at the website http://snia.dga.cl/BNAConsultas/.

2 DInSAR processing THROUGH Esa's g-pod service

During the first year of HAMMER Project we tested the ESA service named Grid Processing On-Demand G-POD (http://gpod.eo.esa.int/) in order to obtain the ground deformation and velocity maps with associated time series for the Grange Orgiera landslide and the Valle d'Aosta Region (Northern Italy). This service implements the Parallel-SBAS processing chain (Casu et al., 2014) and exploits data stored on the Virtual Archive 4 (http://eo-virtual-archive4.esa.int/, in the framework of Supersite initiative). G-POD is accessible through a user-friendly web-interface, and allows setting easily some useful input parameters for processing (e.g., selection of temporal range, baseline and coherence thresholds set, reference point selection). The G-POD service also was exploited to obtain ground deformation, velocity maps and time series in the Atacama Desert test area. This activity, begun in the first year of the Project, is still on going.

In test site of Grange Orgiera Surface deformation map has been obtained by processing 21 ASAR-Envisat images (ascending orbit) spanning from April 2005 to October 2010. The mean velocity map (Figure 7) shows the distribution of the ground deformation in the investigated area, and for each coherent point the displacement time series is also available. The data have been compared to the Envisat data available on the *Piano di Telerilevamento Straordinario* (http://www.pcn.minambiente.it/viewer/) elaborated with the PInSAR technique. The ground deformation distribution and the mean velocity values were comparable.

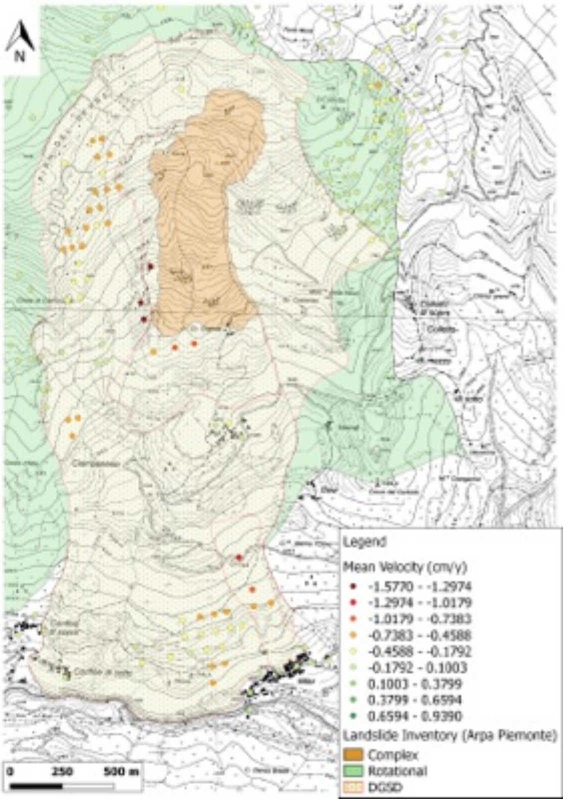

Fig. 7. Mean velocity map obtained by SBAS technique with G-POD service for the Grange Orgiera test site.

In order to analyse the ground deformation time series and their possible trend in Valle d'Aosta, 39 ASAR-Envisat images in ascending orbit, spanning the period from June 2004 to October 2010 were processed. The obtained mean velocity map (Figure 8) shows the ground deformation distribution for most of the region. We focused on the sector between the Champorcher Valley and the principal Valley close to Chatillon (red line in Figure 8) where rock glaciers are present. In order to analyse the ground deformation time series and their eventual trend related to these phenomena, the SBAS point distribution has been compared to the rock glacier polygons (Figure 9) available from the Glaciers Inventory of the Valle d'Aosta Region (http://catastoghiacciai.regione.vda.it/Ghiacciai/MainGhiacciai.html).

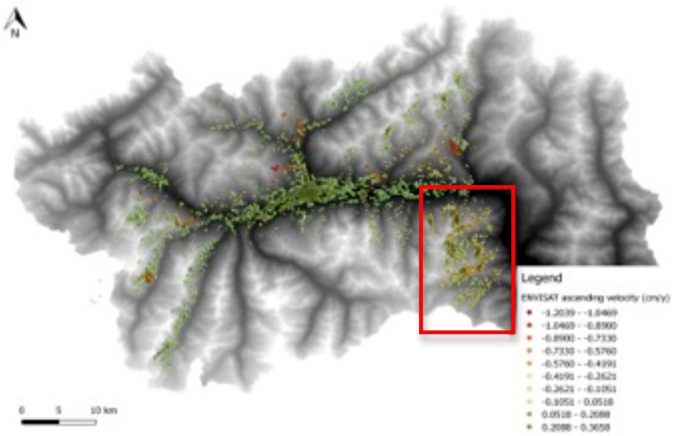

Fig. 8. Mean velocity map obtained by SBAS technique with G-POD service for the Valle d'Aosta Region test site. For this process are considered the Envisat data, composed by 39 images in ascending orbit for the period from June 2004 to October 2010. The red line shows the sector of interest.

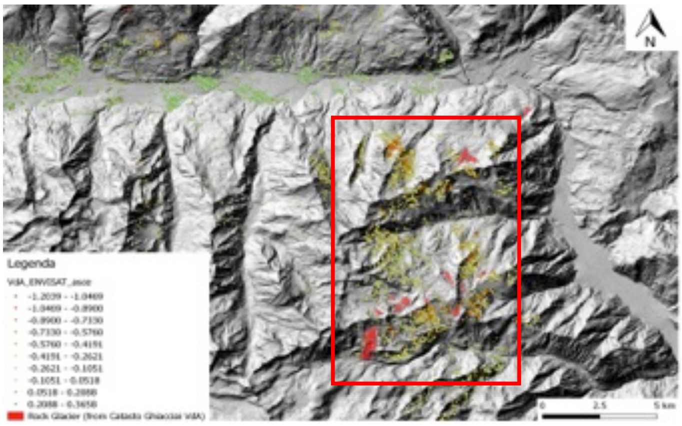

Fig. 9. Mean velocity map (cm/y) obtained by SBAS technique with G-POD service in the territory between Champorcher Valley and the principal Valley, close to Chatillon (red line in Figure 8). The ground deformation distribution observed by SAR data elaboration has been compared with the rock glacier polygons (light red polygons), available from the Glaciers Inventory of the Valle d'Aosta Region.

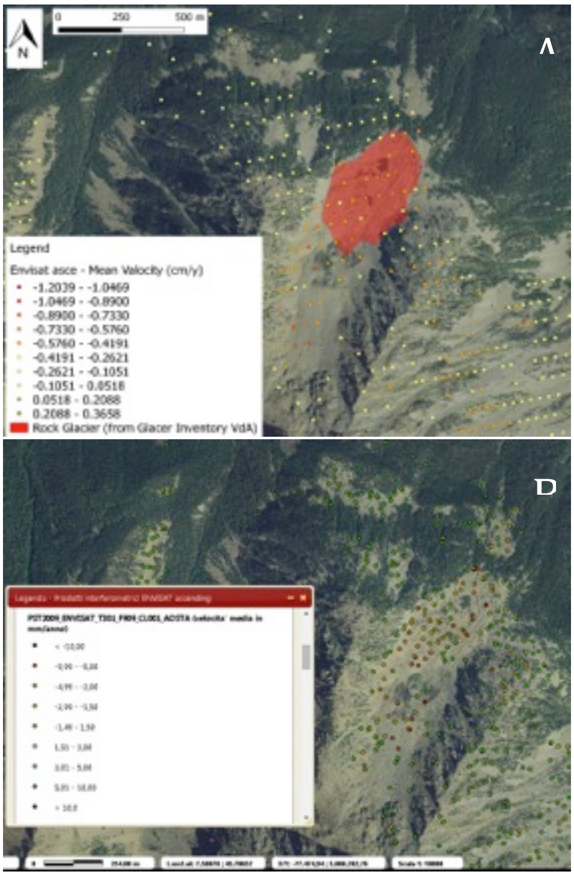

Fig. 10. La Clapey Gerbioz rock glacier; (A) ground deformation distribution obtained with SBAS technique by G-POD service, for ASAR-Envisat satellite, for the period 2004-2010; (B) ground deformation distribution showed on *Piano di Telerilevamento Straordinario* (http://www.pcn.minambiente.it/viewer/) obtained with PSInSAR technique for ASAR-Envisat satellite, for the period 2004-2010.

Figure 10 shows a detail of Clapey Gerbioz rock glacier, where the deformation is concentrated at the right lobe of the rock glacier. The SAR data obtained through G-POD have been also compared with the SAR measurements available on Portale Cartografico Nazionale, elaborated with PSInSAR technique for ASAR-Envisat dataset. The inspection of the *Piano di*

Telerilevamento Straordinario (http://www.pcn.minambiente.it/viewer/) confirmed that the deformation is concentrated at the right lobe of the rock glaciers.

3 FTP strucTure

The implementation of a database to store the collected time series is one of the objectives of HAMMER, as well as the preparation and delivery of the collected information for the NextData main portal. For this purpose during the first year the following actions were set up:

- a metadata schema was prepared as excel file according to European directive INSPIRE (http://essi-lab.eu/do/view/GIcat/InspireMetadata) and according to the different data type (in-situ, SAR, meteorological/climate data), in order to make available the data to the NextData Project (http://geonetwork.evk2cnr.org). For each dataset we compiled a corresponding metadata form that describes the dataset.
- an FTP site (host: s1irpito.to.cnr.it, following authentication) was implemented to store and share data and metadata. The FTP structure, for each test site, is organized as follows:
    - DATA: the folder contains "*in situ* data" and the corresponding "metadata".
    - METEOROLOGICAL DATA: the folder contains meteorological/climate data available for free download on regional website. A specific criteria was adopted to store and share this type of information; the meteorological data will be uploaded in case of data processing, otherwise up to this phase, will be uploaded only the information relate to the type of data available and the website link.
    - ORTOPHOTO: the folder contains the orthophoto maps as tiff files where available, or the link to the regional portal providing the Web Map Service (WMS).
    - PROJECT: the folder contains the Project files prepared for the production of digital map using QGIS software (http://www2.qgis.org/it/site/).
    - SAR: the folder collects the results of Differential Interferometric Synthetic Aperture Radar (DinSAR) processing already available for the test sites.
    - SHP: the folder contains punctual, linear and polygonal shape files of available data for each test sites.
    - TOPOGRAPHY: the folder contains topographic map as tiff files where available, or the link to the regional portal providing the Web Map Service (WMS).

4 Literature review

One of the HAMMER expected results is the analysis of the scientific and technical literature to determine where quantitative surface and sub-surface information on ground deformations in landslide areas is available, and for which periods. For the purpose we compiled a database of scientific and technical papers. An Excel file was produced; the file lists 110 records (i.e. bibliographic documents) classified based on different criteria (Table 2).

Tab. 2. The HAMMER review database schema.

<table>
<tr><th>Name</th><th>Description</th></tr>
<tr><td>ID</td><td>Progressive number</td></tr>
<tr><td>DATA RELATIONSHIP</td><td>Relationship between different types of data</td></tr>
<tr><td>ARTICLE CATEGORY</td><td>Publication type</td></tr>
<tr><td>ARTICLE TOPIC</td><td rowspan="3">General information</td></tr>
<tr><td>AUTHOR</td></tr>
<tr><td>TITLE</td></tr>
</table>

JOURNAL/VOLUME	
YEAR	
ARTICLE TYPE	
PHYSIOGRAPHIC ENVIRONMENT	Mücher et al., 2009 / ISPRA AMBIENTE
CLIMATIC ZONE	Kottek et al., 2006
REGION	
NATION	Geographic location
LAT/LONG	
TEST SITE	
OBSERVATION TYPE	
DATA TYPE	
AREA EXTENSION	Data description
DIRECTION	
THOPOGRAPHIC GRADIENT VARIATION	
LAND USE	

5 Bibliography

BERNARDINO P., FORNARO G., LANARI R., SANSOSTI E., (2002): A new algorithm for surface deformation monitoring based on small baseline differential SAR interferograms. *IEEE Trans. Geosci. Sens.* 40 (11), 2375-2382.

BURDA J., HARTVICH F., VALENTA J., SMÌTKA V. AND RYBÁŘ J., (2013): Climate-induced landslide reactivation at the edge of the Most Basin (czech Republic) – progress towards better landslide prediction. *Nat. Hazards Earth Syst. Sci.*, 13, 361-374, DOI: 10.5194/nhess-13-361-2013.

CALÒ F., ARDIZZONE F., CASTALDO R., LOLLINO P., GUZETTI F., LANARI R., ANGELI M-G., PONTONI F., MANUNTA M., (2014): Enhanced landslide investigations through advanced DInSAR techniques: the Ivancich case stuty, Assisi, Italy. *Remote Sensing of Environment* ,142, 69-82.

CROSTA G.B., DI PRISCO C., FRATTINI P., FRIGERIO G., CASTELLANZA R., AGLIARDI F., (2013): Chasing a complete understanding of the triggering mechanisms of a large rapidly evolving rockslide. *Landslide,* 11, 747-764. DOI:10.1007/s10346-013-0433-1.

CROZIER M.J., (2010): Deciphering the effect of climate change on landslide activity: A review. *Geomorphology,* 124 (3-4), 260-267. DOI: 10.1016/j.geomorph.2010.04.009.

GIORDAN D., ALLASIA P., MANCONI A., BALDO M., SANTANGELO M., CARDINALI M., CORAZZA A., ALBANESE V., LOLLINO G., GUZZETTI F., 2013. Morphological and kinematic evolution of a large earthflow: The Montaguto landslide, soutern Italy. *Geomorphology,* 187 (1): 61-79.

HERRERA G., GUTIÉRREZ F., GARCÍA-DAVALILLO J.C., GUERRERO J., NOTTI D., GALVE J.P., FERNÁNDEZ-MERODO J.A. & COOKSLEY G., (2013): Multi-sensor advanced DInSAR monitoring of very slow landslides: the Tena Valley case study (Central Spanish Pyrenees). *Remote Sensing of Environment,* 128, 31-34.

HUGGEL C., CLAGUE J.J., KORUP O., (2012): Is climate change responsible for changing landslide activity in high mountains? *Earth Surf. Process. Landform,* 37: 77-91.

KOTTEK M., GRIESER J., BECK C., RUDOLF B. AND RUBEL F., (2006): World Map of the Köppen-Geiger climate classification updated. *Meteorologische Zeitshrift*, Vol 15, No. 3, 259-261.

LOLLINO G., ARATTANO M., ALLASIA P AND GIORDAN D., (2006): Time response of a landslide to meteorological events. *Nat. Hazards Earth Syst. Sci.,* 6: 179-184.

MÜCHER C.A., KLIJN J.A., WASCHER D.M. AND SCHAMINÉE J.H.J., (2009): A new European Landscaper Classification (LANMAP): A transparent, flexible and user-oriented methodology to distinguish landscapes. *Ecological Indicators,* 10: 87-103.